

1 **What caused the interdecadal shift of the ENSO impact** 2 **on dust mass concentration over northwestern South Asia?**

3 Lamei Shi ^{1,2}, Jiahua Zhang ^{1,2}, Da Zhang ^{1,2}, Jingwen Wang ^{1,2}, Xianglei Meng², Yuqin
4 Liu³, Fengmei Yao²

5 ¹Key Laboratory of Digital Earth Science, Aerospace Information Research Institute, Chinese Academy
6 of Sciences, Beijing 100094, China

7 ²College of Earth and Planetary Sciences, University of Chinese Academy of Sciences, Beijing 101407,
8 China

9 ³Key Laboratory of Urban Environment and Health, Institute of Urban Environment, Chinese Academy
10 of Sciences, Xiamen 361021, China

11 *Correspondence to:* Jiahua Zhang (zhangjh@radi.ac.cn)

12 **Abstract.** The changes of large-scale circulation, especially El Niño-Southern Oscillation (ENSO), have
13 significant impacts on dust activities over the dust source and downwind regions. However, these impacts
14 present an interdecadal pattern and it remains less clear that which factors lead to the interdecadal
15 variability of the ENSO impact on dust activities over the northwestern South Asia, although previous
16 studies have discussed the response of the interannual dust activities over the northwestern South Asia
17 to the ENSO cycle. Based on the linear regression model and MERRA-2 atmospheric aerosol reanalysis
18 data, this study investigated the interdecadal variability of the ENSO impact on dust activities as well as
19 the associated possible atmospheric drivers under two different warming phases over the northwestern
20 South Asia. Results indicated that the relationship between ENSO and Dust Column Mass Density
21 (DUCMASS) experienced an obvious shift from the accelerated global warming period (1982–1996) to
22 the warming hiatus period (2000–2014). The change of Atlantic and Indian ocean sea surface temperature
23 anomaly (SSTA) pattern weakened the impact of ENSO on dust activities over the northwestern South
24 Asia during 1982–1996, while the change of PDO strengthened ENSO’s effect when it was in phase with
25 ENSO. Both the Atlantic and Indian Ocean SSTA patterns were modulated by the duration of ENSO
26 events (i.e., continuing and emerging ENSO). This study provides new insights to numerical simulation
27 involving the influence of atmospheric teleconnections on the variability of dust activities and their
28 influence mechanisms.

29 **Keywords:** Surface dust mass concentration; ENSO–DUCMASS relationship; interdecadal change;

30 large-scale atmospheric circulation; northwestern South Asia

31 **1 Introduction**

32 Dust aerosols are attracting an increasing concern due to its adverse impacts on human health (Chen
33 et al., 2004; Bozlaker et al., 2013; Erel et al., 2006; Kaiser and Granmar, 2005; Poulsen et al., 1995;
34 Sanchez de la Campa et al., 2013; Schulz et al., 2012) and environmental problems (Avila, 1998; Razakov
35 and Kosnazarov, 1996; Behrooz et al., 2017). Dust aerosols can also influence the earth's radiation budget
36 balance and climate change through direct and indirect effects (Mahowald et al., 2014; Miller and Tegen,
37 1998). Dust aerosols can reflect incoming solar radiation and cool the surface, which is known as the
38 direct effects (Mahowald et al., 2006; Tegen et al., 1996); they can also affect the cloud droplet size,
39 cloud albedo and lifespan by forming into cloud condensation nuclei and ice nuclei, which is known as
40 the indirect effects (Hansen et al., 1997). The Northwest Indian subcontinent, which is the most arid and
41 semiarid area of South Asia, suffers heavy and frequent dust storms in summer due to extremely dry
42 climate and strong winds (Jin and Wang, 2018). Those dusts can travel long-distance to North India and
43 the Arabian Sea, degrading air quality (Mahowald et al., 2010) and modifying ocean biogeochemistry
44 processes (Richon et al., 2018; Singh et al., 2008). Particularly, dust aerosols can change local radiation
45 budget, circulations, and Indian summer monsoon rainfall through absorption and scattering of solar
46 radiation (Wu et al., 2018; Jin et al., 2021; Mahowald et al., 2006; Tegen et al., 1996). The mineral dust
47 over the northwestern South Asia is closely associated with the long-term variation of global climate
48 (Bollasina et al., 2011; Jin et al., 2018; Banerjee et al., 2019). To better understand such feedback, and
49 give early warning to reduce disasters and losses caused by dust events, it is important to find out the
50 controlling factors of the Dust Column Mass Density (DUCMASS) and its long-term variation.

51 ENSO, as a periodic fluctuation in sea surface temperature (SST) and the air pressure across the
52 equatorial Pacific Ocean, is as the primary large-scale driver of dust loading over the global dust source
53 region (Trenberth et al., 2014). Prospero and Nees (1986) found that ENSO-related large-scale
54 atmospheric circulation changes led to the increase in winter dust concentration over North Africa. Xi
55 and Sokolik (2016a) indicated that in La Niña years, the precipitation and soil moisture over Central Asia
56 decreased and caused poor vegetation conditions and heavy drought conditions, which strengthened dust

57 activities. Yu et al. (2015b) suggested that La Niña events provided favorable conditions for dust
58 activities over Saudi Arabia. However, Banerjee et al. (2016) proposed that the low-level southwesterly
59 winds and high-level westerly winds accompanied with La Niña events were the main factor that
60 contributed to the elevated dust levels over the Arabia Peninsula. Abish and Mohanakumar (2013)
61 pointed out that strengthened westerly circulation related with El Niño increased the dust transmission
62 from the Middle East to the Indian subcontinent. Simultaneously, the impacts of ENSO on dust activities
63 were also modulated by other atmospheric factors, e.g., PDO could strengthen the effect of ENSO when
64 it was in phase with ENSO (He et al., 2013; Wang et al., 2008; Wang et al., 2014); the spring dust index
65 over the northern China in the years when negative AO and El Niño occurred synchronously was
66 significantly higher than that in the years when positive AO and La Niña were concurrent (Liu et al.,
67 2020; Lee et al., 2015); IOD could also influence the dust activities over the northwestern Indian ocean
68 by adjusting the El Niño related water vapor conditions (Banerjee and Kumar, 2016).

69 ENSO exhibits profound impacts on the global climate. Nevertheless, the Earth climate is varying
70 and ENSO, including its feedback and influences on the changing global climate, also experience
71 significant changes (Yang and Jiang, 2014; Yuan and Yang, 2012; Weng et al., 2007; Weare et al., 1976;
72 Yu and Kao, 2007; Ashok et al., 2007). In the mid-1970s, an interdecadal climate regime shift was
73 observed in the large-scale boreal winter circulation pattern over the North Pacific (Graham, 1994; Nitta
74 and Yamada, 1989; Trenberth and Hurrell, 1994). Another remarkable climate change was observed in
75 the early 21st century, i.e., an accelerated global warming prevailed before late 1990s and a warming
76 hiatus dominated after that (Easterling and Wehner, 2009; Fyfe et al., 2011, 2013). After 2013, the global
77 warming hiatus came to an end due to a persistent warm condition over the equatorial Pacific between
78 Mar. 2014 and May 2016 (Hu and Fedorov, 2017). Concurrent with the Pacific climate shift, the large-
79 scale circulation pattern and their atmospheric teleconnection also exhibited an interdecadal change, e.g.,
80 the correlation between El Niño and rainfall over India turned to be insignificant from the late 1970s,
81 simultaneously, the relationship between ENSO and monsoon also weakened around this turning point
82 (Kumar et al., 1999). Two influence mechanisms were proposed to explain this weakened ENSO–
83 monsoon relationship. One was the varied location of Walker circulation that adjusted the monsoon
84 rainfall over Indian region, the other was the temperature change over Eurasia that modulated the land-

85 sea thermal gradient. Besides, the impact of Atlantic Ocean pattern on the monsoon circulation over the
86 Indian Ocean became stronger since late 1970s as the influence of the tropical Pacific has reduced
87 (Srivastava et al., 2019; Sabeerali et al., 2019; Kucharski et al., 2007). This in-turn impacted the
88 circulation responsible for dust uplift and transport.

89 It was reported that the effect of ENSO on Indian summer monsoon rainfall (ISMR), which was an
90 important modulator to DUCMASS, experienced a remarkable interdecadal change and many factors
91 may cause this transition (Yang and Huang, 2021). Till now, the interdecadal variability in the links of
92 DUCMASS over the northwestern South Asia with ENSO has not been fully investigated, as compared
93 to the North African and West Asian counterpart (Yu et al., 2015). In addition, though many factors have
94 been proved to influence the short-term (e.g., interannual scale) variation of the relationship between
95 ENSO and dust activities over South Asia, their effects on the long-term (e.g., interdecadal scale) change
96 are still unclear. Cai et al. (2014) pointed out that global warming will have a significant impact on ENSO.
97 The extreme El Niño events will become more frequent under the changes of atmospheric convection in
98 the next half of the 21st century. Thus, understanding the physical mechanism of the shifting ENSO–
99 DUCMASS relationship is of profound implications for the forecast of dust trend in the future climate
100 change scenario. This study aims to investigate the large-scale atmospheric factors that contribute to the
101 interdecadal variability of the ENSO impact on DUCMASS over the northwestern South Asia.

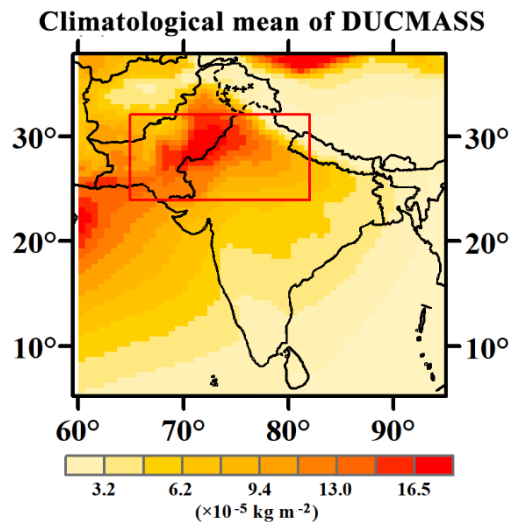
102 The paper is organized in the following structure: section 2 describes the datasets and methods;
103 section 3 presents factors that influence the interdecadal change of the relationship between DUCMASS
104 and wintertime Niño-3 index; section 4 discusses the deficiency and prospect of this study, and the
105 conclusions are given in section 5.

106 **2 Data and methods**

107 **2.1 Study area**

108 The main dust source over South Asia is a large arid region in the northwestern part of the Indian
109 subcontinent, which stretches from India to Pakistan. Most of the dust aerosols over this region come
110 from the Thar desert. The southeastern part of the Thar desert lies between the Aravalli Hills. The desert
111 extends as far as the Punjab Plain in the north and northeast, the alluvial plains of the Indus River in the

112 west and northwest, and the Great Rann of Kutch along the western coast. The desert presents an
 113 undulating surface, with high and low sand dunes separated by sandy plains and low barren hills. The
 114 soils are mainly consisted by desert soils, red desertic soils, sierozems, the red and yellow soils of the
 115 foothills, the saline soils of the depressions, and the lithosols (shallow weathered soils) and regosols (soft
 116 loose soils) found in the hills. The subtropical desert climate here results from persistent high pressure
 117 and subsidence. The prevailing southwest monsoon winds from Indian Ocean that bring rain to much of
 118 the Indian subcontinent in summer tend to bypass the Thar to the east. The soils are generally infertile
 119 and overblown with sand due to severe wind erosion (Augustyn et al., 2019). The amount of annual
 120 rainfall in the desert is low, ranging from about 100 mm or less in the west to about 500 mm in the east.
 121 Almost 90 % of the annual rainfall occurs in the season southwest monsoon, from July to September.
 122 While the prevailing wind is dry northeast monsoon during other seasons. Dust storms and dust-raising
 123 winds are common from May to July (Chauhan, 2003). Thus, the DUCMASS used in this study is
 124 averaged from June to July and May is neglected to eliminate the disturbance of seasonal climatological
 125 differences. Analysis is carried out over the dust source in the northwestern South Asia (65° – 82° E, 24° –
 126 32° N), as shown in Fig. 1. All variables involving spatial average are taken from this region unless stated
 127 otherwise.



128
 129 **Figure 1: Climatological mean DUCMASS over South Asia based on the MERRA-2 dataset. The dust source**
 130 **over the northwestern South Asia is marked with red rectangle.**

131 **2.2 Datasets**

132 **2.2.1 Dust concentration**

133 Dust column mass density from 1982 to 2014 was obtained from the Modern-Era Retrospective
134 Analysis for Research and Applications, version 2 (MERRA-2). MERRA-2 is produced via the Goddard
135 Earth Observing System-Data Assimilation System (GEOS-DAS, version 5.12.4) based on GEOS-5
136 climate model and the Gridpoint Statistical Interpolation (GSI) analysis scheme (Gelaro et al., 2017).
137 Extensive satellite data are integrated into MERRA-2 to estimate dust concentration (Veselovskii et al.,
138 2018; Randles et al., 2017). The dust products were comprehensively validated using the results of
139 ground-based observation, satellite measurements, and numerical simulation (Buchard et al., 2017;
140 Randles et al., 2017). They have been widely applied to researches on global environment and climate
141 change (He et al., 2019; Randles et al., 2017). The variable “Dust Column Mass Density-PM_{2.5}”
142 (DUCMASS25) with a spatial resolution of 0.625°×0.5° (longitude×latitude) used in this study is from
143 the dataset of “avgM_2d_aer_Nx”. The time series of DUCMASS25 dataset was compared with that of
144 DUCMASS dataset, to find that the time series of DUCMASS25 and its association with Niño index
145 showed the same change pattern with that of DUCMASS. Only the results acquired by DUCMASS25
146 were presented in this study.

147 **2.2.2 Land and sea surface temperature**

148 To explore the possible influence of SST on the South Asian dust activity, we used three SST
149 datasets from 1981 to 2014 for comparison: (1) The National Oceanic and Atmospheric Administration
150 (NOAA) Extended Reconstructed SST (ERSST) version 5 (Huang et al., 2017) that is available at 2°×2°
151 spatial resolution is used for analysis, (2) Centennial in situ Observation-Based Estimates (COBE)
152 version 2 SST data at 1°×1° spatial resolution (Hirahara et al., 2014) and (3) Hadley Centre Global Sea
153 Ice and Sea Surface Temperature (HadISST1.1) dataset produced by the Met Office, starting from 1870
154 up to the present with a horizontal resolution of 1°×1° (Rayner et al., 2003). While the land-sea thermal
155 contrast was calculated from the Hadley Centre Climate Research Unit Temperature version 5.0.1.0
156 (HadCRUT5) data from 1981 to 2014, which is a blend of the Climatic Research Unit land-surface air
157 temperature dataset (CRUTEM5) and the Hadley Centre sea-surface temperature (HadSST4) dataset
158 (Osborn et al., 2021). The longitude and latitude of SST index involved in this study were shown in Table
159 1.

160 **Table 1: Longitude and latitude of SST index used in this study.**

Acronyms	Full Name	Longitude and Latitude	Involved Ocean
Niño-3	—	150°–90° W, 5° S–5° N	Pacific
Niño-3.4	—	170°–120° W, 5° S–5° N	Pacific
Niño-4	—	160° E–150° W, 5° S–5° N	Pacific
ASGI	Atlantic SSTA gradient index	North: 60°–30° W, 0–20° N South: 20° W–10° E, 0–20° S	Atlantic Ocean
TWISSTA	Tropical western Indian ocean SSTA	50°–70° E, 10° S–15° N	Indian Ocean
IOD	Indian Ocean Dipole	West: 50°–70° E, 10° S–10° N East: 90°–110° E, 10° S–0°	Indian Ocean
PDO	Pacific decadal oscillation	117.5° E–77° W, 20°–66.5° N	Pacific

161 **2.2.3 Large-scale climate indices**

162 Three monthly Niño indices Niño-3, Niño-3.4, and Niño-4 from 1981 to 2014, which monitor the
 163 SST anomalies averaged across the eastern equatorial Pacific, Pacific from dateline to the South
 164 American coast, and central equatorial Pacific, respectively, were used to analyze their links with
 165 DUCMASS over the northwestern South Asia. Kinter et al. (2002) pointed out that Nov.–Jan. is the peak
 166 season for El Niño/La Niña, thus the average Niño index from (–1) Nov. to (0) Jan. was used. Only one
 167 Niño index that showed the highest correlation coefficient was retained in this study, i.e., Niño-3. The
 168 time series of ENSO was represented by Niño-3 and Niño-3 also referred to ENSO. The large-scale
 169 climate indices, such as PDO and IOD, was also used to explore the potential factors that contributed to
 170 the interdecadal shift of ENSO–DUCMASS relationship. All those indices were from the Climate Predict
 171 Center of National Oceanic and Atmospheric Administration (NOAA/CPC).

172 **2.3 Method**

173 In this study, we compared the impact of ENSO on DUCMASS over the northwestern South Asia
 174 under two different warming epochs, and investigated the potential global change drivers to the shift of
 175 ENSO–DUCMASS relationship. The global warming was separated into the accelerated warming period
 176 from 1982 to 1996 (P1) and the warming hiatus period from 2000 to 2014 (P2). The year 2014 was added

177 to the warming hiatus period to keep the length of those two periods consistent. This classification was
178 not controversial since the ENSO year stated in this study spanned from antecedent November to current
179 January.

180 **2.3.1 Contribution of factors to relationship**

181 The contribution of X (Indian Ocean SSTA, Atlantic SSTA gradient index, and PDO) modifying
182 ENSO–DUCMASS relationship was defined as: sliding regression of X onto Niño-3 index multiplies by
183 sliding regression of DUCMASS onto X with Niño-3 removed (Yang and Huang, 2021).

184 **2.3.2 Signal removal method**

185 The ENSO signals were removed from the oceanic SSTA pattern when analyzing spatial coupling
186 and regression mode between the oceanic SSTA pattern and DUCMASS as well as local surface
187 conditions (precipitation, soil moisture, land cover, wind, etc). Simultaneously, the oceanic SSTA signals
188 were removed from ENSO when calculating the sliding correlation between ENSO and DUCMASS. In
189 this study, the residual time series based on the linear regression method were used to represent the ENSO
190 (or oceanic SSTA index)-independent components (Yang and Huang, 2021), as shown in Eq. (1):

$$\xi_{remove} = \xi - Z \times \frac{cov(\xi, Z)}{var(Z)} \quad (1)$$

191 Where ξ_{remove} is the time series of variable ξ with Z removed, ξ is the time series of original
192 variable, Z is the time series of related signal that needs to be removed, cov indicates the covariance
193 between two variables, and var indicates the variance of ENSO.

194 **2.3.3 Coupled spatial pattern analysis**

195 The maximum covariance analysis (MCA) is a useful tool for isolating the most coherent pairs of
196 spatial patterns and their associated time series by performing an eigenanalysis on the temporal
197 covariance matrix between two geophysical fields (Storch and Zwiers, 1999). The MCA method was
198 used to analyze the coupled patterns between DUCMASS and oceanic SSTA.

199 **2.3.4 Definition of different types of ENSO**

200 Following Yang and Huang (2021), the EM and CT ENSO were defined based on the three-month

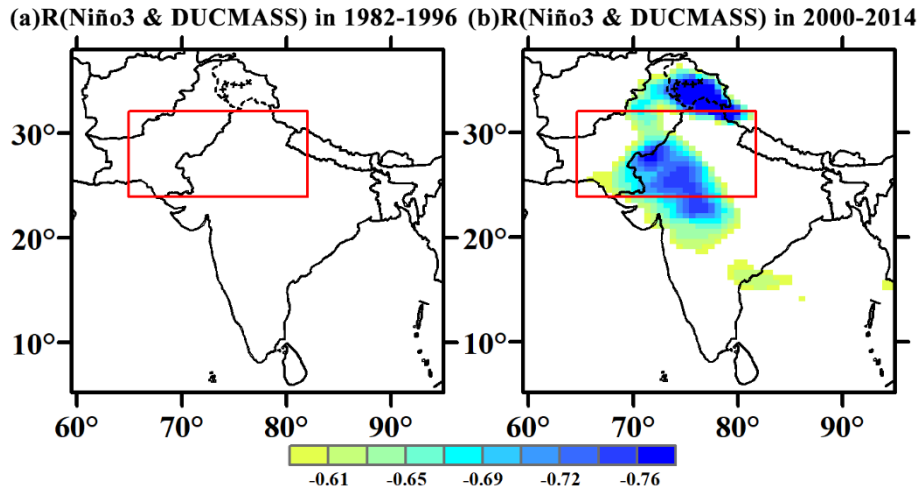
201 running mean of the Niño-3 index. Two situations for the CT ENSO were considered, i.e., the slowly
202 decaying events and the developing events since the previous winter. For the slowly decaying situation,
203 a CT ENSO was identified when the average Niño-3 of (–1) Oct.–(0) Jan. was greater than 0.5 (below –
204 0.5) standard deviation (STD), became greater than 0.5 (below –0.5) STD in single month during (0)
205 Mar.–(0) May, and remained positive (negative) during (0) Jun.–(0) Sep.. For the developing events since
206 the previous winter, a CT ENSO was identified when the Niño-3 was greater than 0.75 (below –0.75)
207 STD in any month from (–1) Oct. to (0) May, accompanied by positive (negative) values for eight single
208 months, and the average Niño-3 of (0) Jun.–(0) Sep. was greater than 0.5 (below –0.5) STD. To acquire
209 more available samples in the study period, all the ENSO years that were not defined as CT ENSO were
210 identified as EM ENSO year in this study, which was different from Yang and Huang (2021). Based on
211 this definition, the CT El Niño years during 1982–2014 included 1982, 1983 and 1987; CT La Niña years
212 included 1984, 1985, 1989, 1996, 1999, 2000, and 2011; EM El Niño years included 1995, 1998, 2003,
213 2005, 2007, and 2010; EM La Niña years included 2008 and 2012.

214 In this study, “(0) month” represented the year concurrent with the year when DUCMASS was
215 acquired and “(–1) month” represented the preceding year.

216 **3 Results**

217 **3.1 Observed interdecadal change of the impact of ENSO on DUCMASS**

218 In the present study, we found that the DUCMASS–Niño-3 relationship experienced an interdecadal
219 transition at around 1999/2000. Based on the 15-year sliding correlation from 1982 to 2014 (Fig. 4 (a)),
220 the DUCMASS–Niño-3 relationship was weak before the early of 2000s and became stronger after that.
221 Specifically, the winter Niño-3 index ((–1) Nov.–(0) Jan.) presented a significant negative relation ($R=-$
222 0.68 , $p<0.01$) with DUCMASS during 2000–2014 (P2), while no significant correlation ($R=-0.41$,
223 $p>0.05$) was observed in 1982–1996 (P1), as shown in Fig. 2.



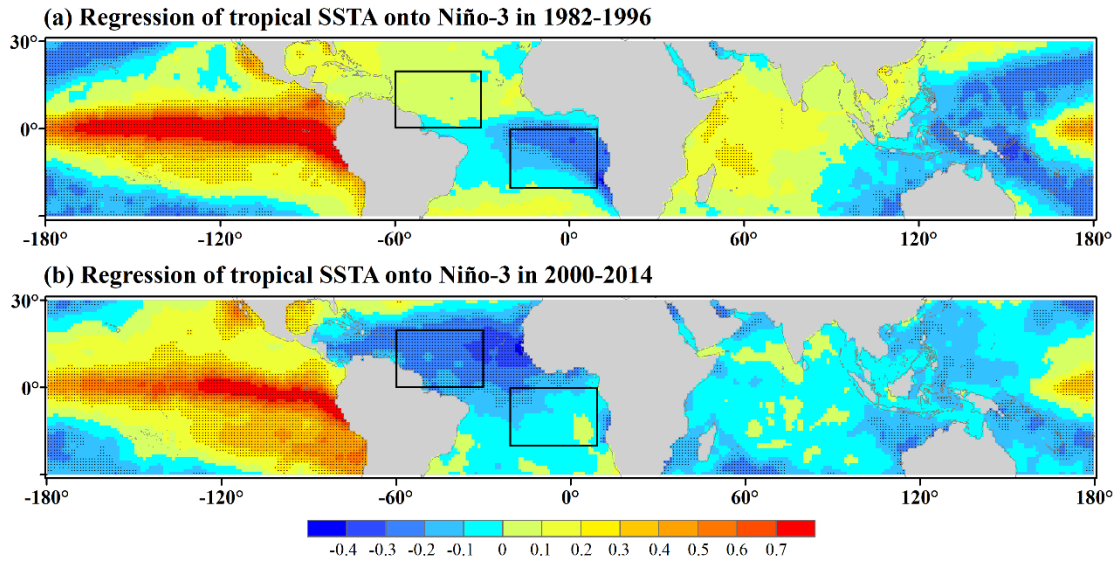
224

225 **Figure 2: Correlation between Niño-3 index and DUCMASS over South Asia during (a) 1982–1996 and (b)**
 226 **2000–2014. (Only correlations that passed the 99% confidence level were presented).**

227 **3.2 Factors influencing the interdecadal change of the impact of ENSO on DUCMASS**

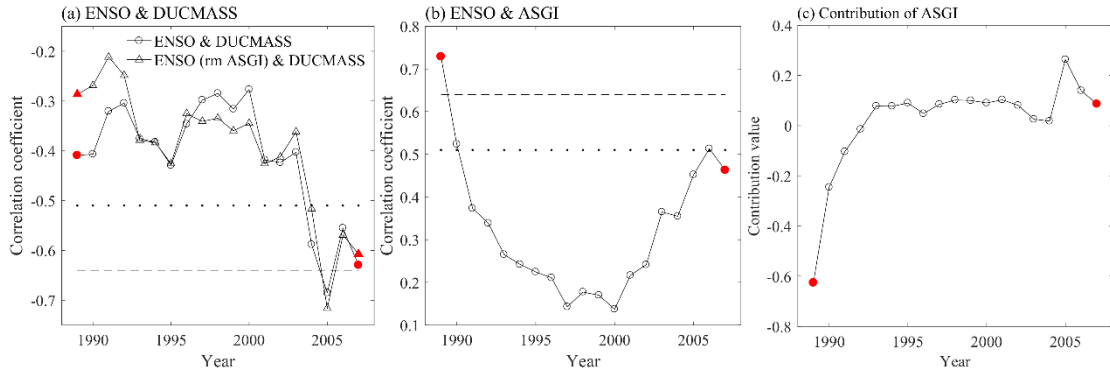
228 **3.2.1 Tropical Atlantic SSTA pattern**

229 With the global climate change observed in early 2000s, the ENSO-related tropical Atlantic SSTA
 230 experienced an obvious transition, i.e., from an Atlantic Niña pattern during 1982–1996 to an Atlantic
 231 Niño pattern during 2000–2014 (Fig. 3), which coincides with the findings of Yang and Huang (2021).
 232 The tropical Atlantic SSTA pattern was a crucial factor for the restoration of ENSO–ISMR relationship
 233 since the late 1990s (Yang and Huang, 2021), thus, it could also disturb the impact of ENSO on dust
 234 activities over the northwestern South Asia. In order to validate the connection between the Atlantic
 235 SSTA and the DUCMASS–Niño-3 relationship, an Atlantic SSTA gradient index (ASGI) was used to
 236 describe the SSTA pattern shift in the tropical Atlantic, which represented the difference of averaged
 237 SSTA between tropical North Atlantic and tropical South Atlantic (marked by two rectangles in Fig. 3).
 238 According to Tokinaga et al. (2019), the Atlantic Niña pattern develops and is most sensitive to ENSO
 239 in spring, thus the SST averaged from Mar. to May was used in this section.



240
 241 **Figure 3: Regression of spring (Mar.–May) tropical SSTA onto Niño-3 index. Black rectangles denote the**
 242 **regions to define ASGI. The range of the upper one is 60–30° W, 0–20° N and that of the lower one is 20° W–**
 243 **10° E, 20–0° S. The black dots represent significance at ≥ 90 % confidence level. (Similar with Fig. 2 (c)–(d) of**
 244 **Yang and Huang (2021) but with different time spans)**

245 The relationship between Niño-3 and DUCMASS witnessed a reversal at the early 2000s,
 246 simultaneously, the correlation between Niño-3 and ASGI exhibited the similar change. The correlation
 247 between Niño-3 and ASGI passed the 99% confidence level during P1, while it did not pass the 95%
 248 confidence level during P2, as shown in Fig. 4 (b). However, the correlation between Niño-3 and
 249 DUCMASS showed a contrary trend with a higher correlation coefficient appeared in P2. Figure 4 (a)
 250 showed that the DUCMASS–Niño-3 relationship was weakened when the ASGI signals were removed
 251 from Niño-3 index during P1, while during P2, the DUCMASS–Niño-3 relationship remained the same
 252 with or without the ASGI signals removed. In addition, the contribution of ASGI to the DUCMASS–
 253 Niño-3 relationship (Fig. 4 (c)) proved that during P1, ASGI weakened this relationship while no
 254 significant contribution was observed during P2. Thus, it is hypothesized that the strengthening
 255 (weakening) of the response of ASGI to Niño-3 weakened (strengthened) the impact of Niño-3 on
 256 DUCMASS during P1 (P2).



257

258

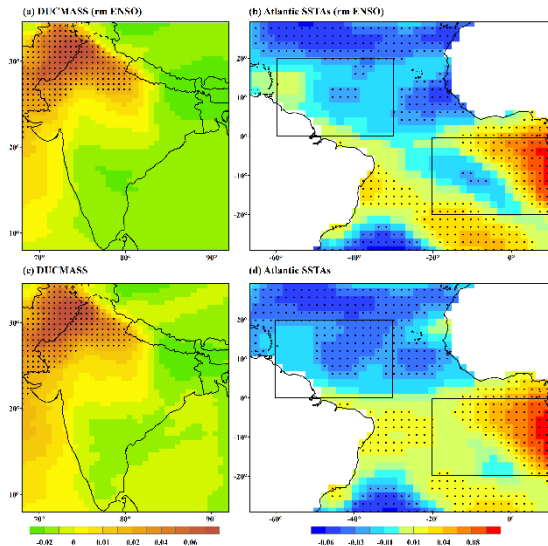
259

260

261

262

Figure 4: (a) The 15-year sliding correlation between DUCMASS and Niño-3 with and without ASGI-related signals removed; (b) 15-year sliding correlation between Niño-3 and ASGI; (c) Sliding contribution of ASGI to DUCMASS–Niño-3 relationship. The two red filled markers represented the 15-year window spanning from 1982 to 1996 and 2000 to 2014, respectively. The x-axis denotes the middle year of the period under analysis.



263

264

265

266

267

Figure 5: Spatial correlation between spring (Mar.–May) tropical Atlantic SSTA and DUCMASS of the first mode of the MCA analysis in 1982–2014. The first MCA mode of (a) the DUCMASS, and (b) the tropical Atlantic SSTA with ENSO-related signals removed. (c)–(d) As in (a)–(b), but for the original series including the ENSO signal. The black dots represent significance at $\geq 90\%$ confidence level.

268

269

270

271

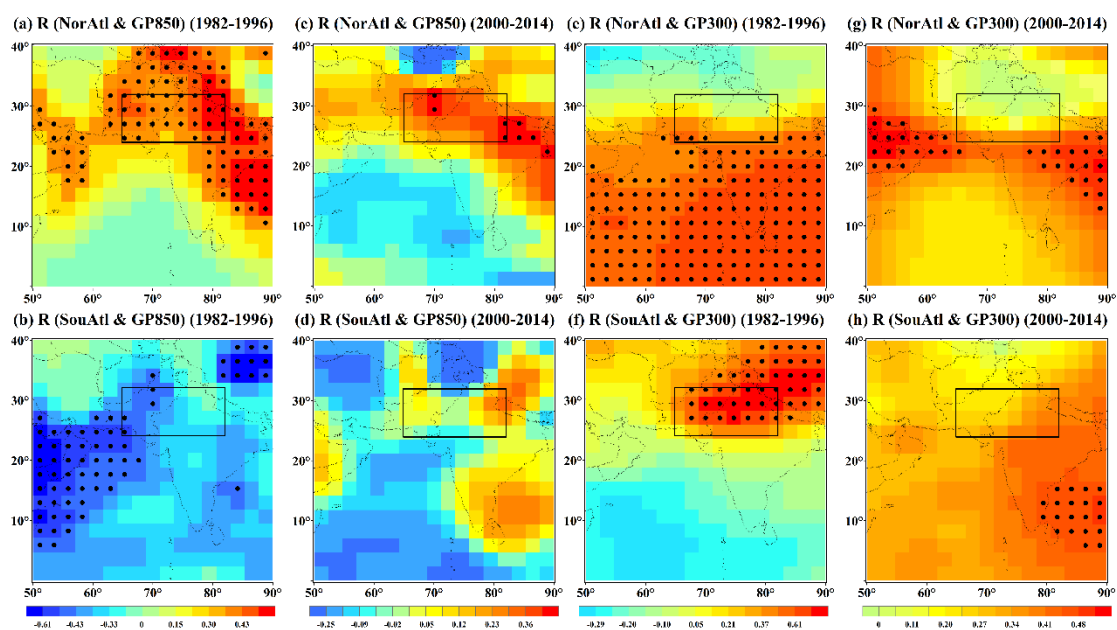
272

273

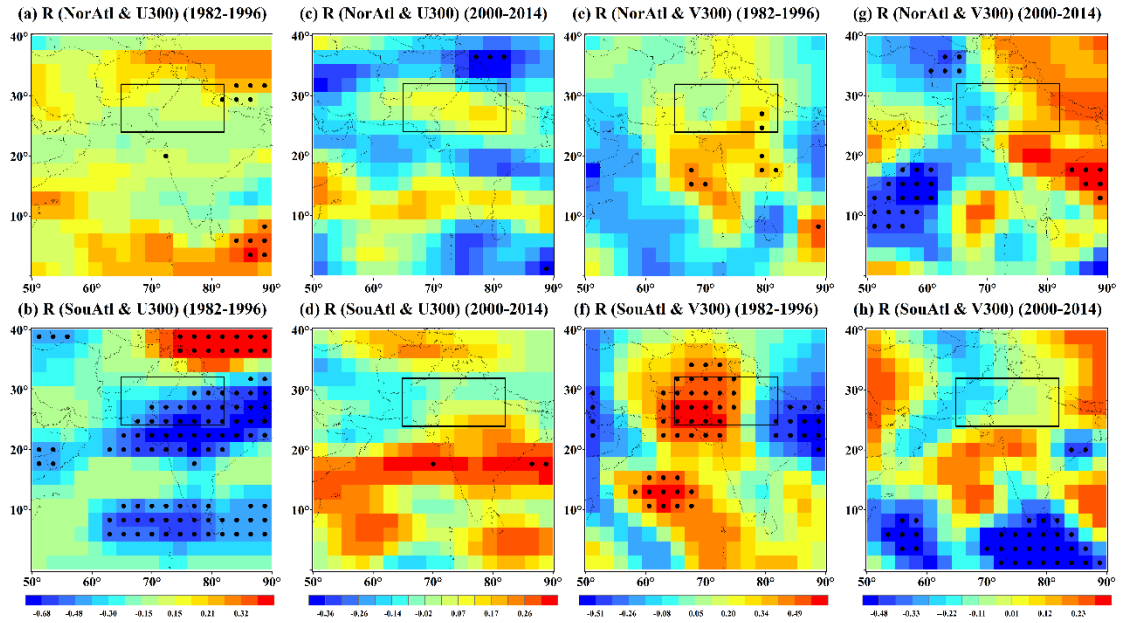
274

In order to validate the effect of Atlantic SSTA pattern on the DUCMASS–Niño-3 relationship, the spatial coupling mode between DUCMASS and tropical Atlantic SSTA was explored. Figure 5 showed that the negative ASGI, i.e., negative SST anomaly over the tropical North Atlantic and positive SST anomaly over the tropical South Atlantic, was coupled with increased DUCMASS over the northern and northwestern India. This pattern was not impacted by ENSO since the MCA results with ENSO-related signals removed were similar with that including the ENSO-related signals, as shown in Fig. 5. Figures 6 and 7 further illustrated the influence mechanism of Atlantic SSTA pattern onto DUCMASS. Figure 6

275 showed that the effect of North and South Atlantic SSTA (NorAtl/SouAtl) with ENSO signal removed
 276 on the geopotential height (GP) at 850hPa/300hPa exhibited significant difference during P1, while they
 277 were close (all are not significant) in P2. Similarly, significant difference was also seen in the effect of
 278 North and South Atlantic SSTA on the zonal/meridional wind (U/V) at 300hPa in P1, which disappeared
 279 in P2, as shown in Fig. 7. This was consistent with the variation of Atlantic SSTA's contribution to
 280 DUCMASS–Niño-3 relationship, i.e., during P1, the Atlantic SSTA pattern was featured with a Niña type
 281 (Fig. 3 (a)), thus the South Atlantic presented stronger influence on the atmospheric circulation over
 282 South Asia, which weakened the impact of ENSO on DUCMASS; while in P2, the negative North
 283 Atlantic SSTA (Fig. 3 (b)) decreased the SSTA gradient between North and South Atlantic and offset the
 284 effect of the Niña pattern, which weakened the response of atmospheric circulation on North and South
 285 Atlantic SSTA gradient and strengthened the DUCMASS–Niño-3 relationship.



286
 287 **Figure 6: Correlation between spring (Mar.–May) tropical North and South Atlantic SSTA (NorAtl/SouAtl)**
 288 **with ENSO signal removed and geopotential height (GP) at 850hPa (a)–(d) as well as 300hPa (e)–(h) in dust**
 289 **season (Jun.–Jul.). (Correlations that passed the 90% confidence level were marked by black dots).**



290

291 **Figure 7: Correlation between spring (Mar.–May) tropical North and South Atlantic SSTA (NorAtl/SouAtl)**
 292 **with ENSO signal removed and zonal wind (U) (a)–(d) as well as meridional wind (V) (e)–(h) at 300hPa in**
 293 **dust season (Jun.–Jul.). (Correlations that passed the 90% confidence level were marked by black dots).**

294

295

296

297

298

299

300

301

302

303

304

305

306

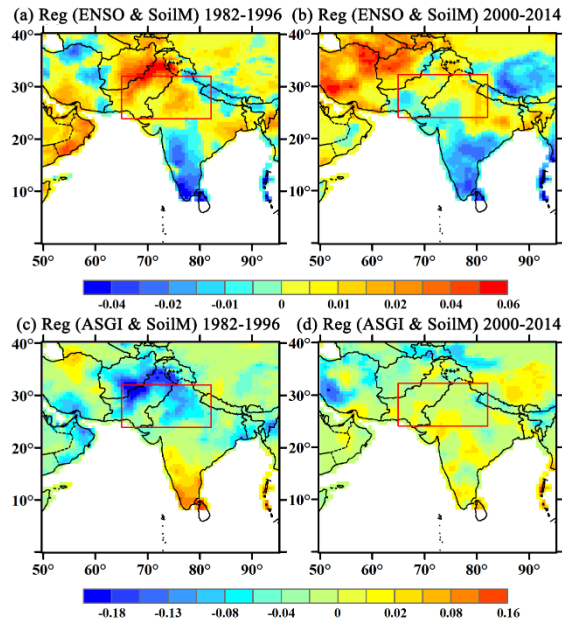
307

308

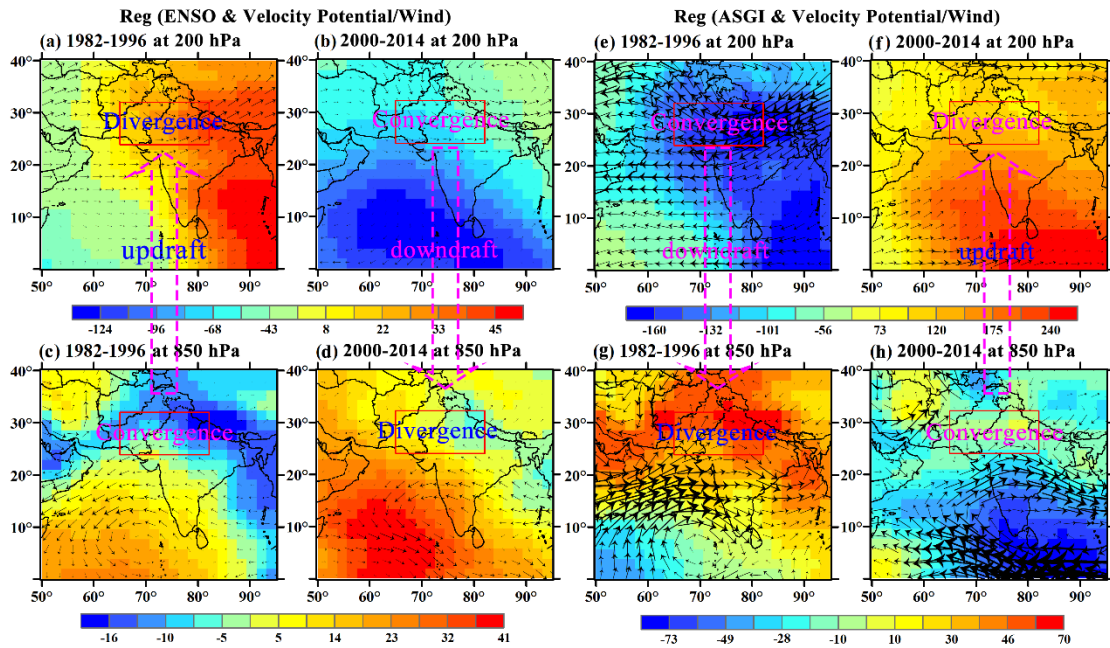
309

In order to verify the inhibitory effect of Atlantic SSTA pattern on the DUCMASS–Niño-3 relationship, we analyzed the regression of ASGI onto the local conditions that directly influenced DUCMASS, such as precipitation (PPT), soil moisture (SoilM), Normalized Difference Vegetation Index (NDVI), and air flow. Figure 8 showed that the regression coefficients between ASGI and SoilM as well as PPT and NDVI (not shown) were opposite to that between Niño-3 and SoilM during P1, while during P2, the abovementioned differences were weakened. Besides, Figure 9 demonstrated that the regression coefficients between Niño-3 and velocity potential (VP) as well as wind field at 200hpa and 850hPa were also contrary to the regression coefficients between ASGI and those factors, indicating the opposite effect of ASGI and ENSO on local wind field and convection. All of those proved the inhibitory effect of Atlantic SSTA pattern on the DUCMASS–Niño-3 relationship during P1. In addition, to further elaborate the physical mechanisms of the interaction between ENSO and dust activities, the composite differences of the abovementioned climatic variables between El Niño and La Niña years as well as that between positive ASGI (ASGI+) and negative ASGI (ASGI-) years were presented, as shown in Figs. S1–S2. Figure S1 showed that the SoilM averaged from June to July in El Niño years exhibited positive anomalies, while that in La Niña years exhibited the reversed anomalies. The differences of SoilM between ASGI+ and ASGI- during P1 were negative, which were contrary to that between El Niño and

310 La Niña conditions, while the differences during P2 reversed compared with those in P1. Simultaneously,
 311 the differences of VP at 200hPa and 850hPa between ASGI+ and ASGI- also presented contrary change
 312 with those between El Niño and La Niña years during P1 and P2, as shown in Fig. S2. The mechanisms
 313 illustrated by the composite difference were analogous with the regression between dust activities and
 314 the climatic variables, both of which clarified the effect of ASGI on the relationship between ENSO and
 315 dust activities over the northwestern South Asian dust source.



316
 317 **Figure 8: (a)–(b) Regression of ENSO with ASGI-related signals removed onto Soilm in dust season (Jun.–**
 318 **Jul.); (c)–(d) Regression of ASGI with ENSO-related signals removed onto Soilm in dust season (Jun.–Jul.).**



319
 320 **Figure 9: (a)–(d) Regression of ENSO with ASGI-related signals removed onto velocity potential (VP) and**

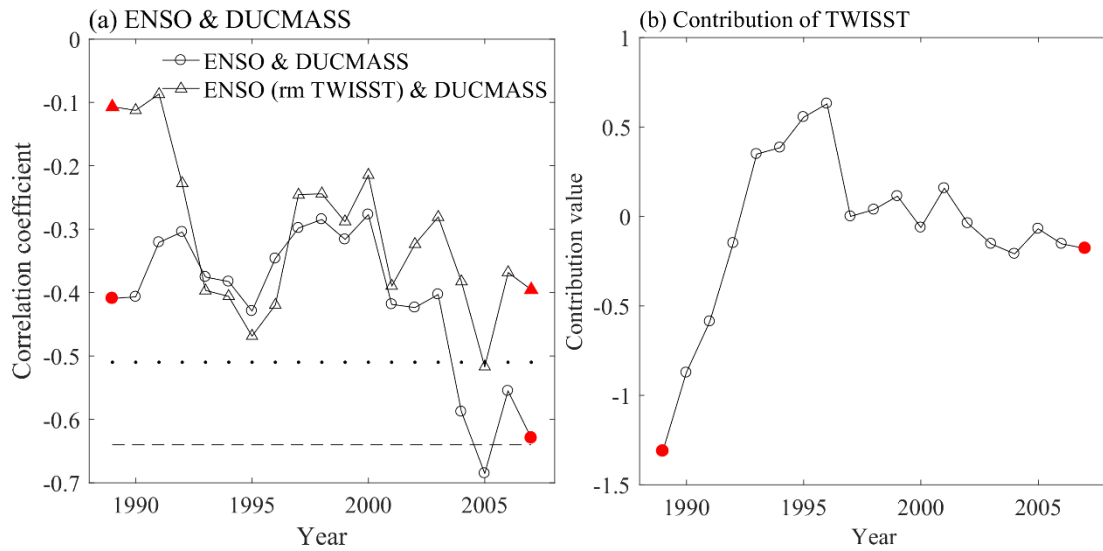
321 wind at 200hPa and 850hPa in dust season (Jun.–Jul.); (e)–(h) Regression of ASGI with ENSO-related signals
322 removed onto velocity potential and wind at 200hPa and 850hPa in dust season (Jun.–Jul.).

323 3.2.2 Tropical Indian ocean SSTA pattern

324 This study explored the effect of Indian ocean SSTA pattern on the DUCMASS–Niño-3 relationship.
325 The covariability between the western Pacific and Indian Ocean has been widely recognized by previous
326 studies (Kug et al., 2005; Wang et al., 2003; Watanabe and Jin, 2002). ENSO can affect the Indian Ocean
327 SST in the form of Walker circulation and the Indian Ocean variability can also modulate the ENSO
328 variability (Wu and Kirtman, 2004; Yu et al., 2002; Kug et al., 2005). It is known that ENSO mainly
329 influences the monsoon rainfall of South Asia through changing the SST of Indian ocean (Krishnamurthy
330 and Kirtman, 2003; Srivastava et al., 2019). Du et al. (2009) indicated that the North Indian Ocean
331 warming displayed two peaks in Nov.–Dec.(–1) and Jun.–Aug.(0), with the second peak larger in
332 magnitude. Cherchi and Navarra (2013) also pointed out that the connection between ISM and Indian
333 ocean SST pattern was mostly confined in summer and autumn. Besides, compared to Atlantic, the Indian
334 ocean is closer to the South Asian dust source, thus it takes less time to transmit the signal (partially
335 through wave train propagation) from the Indian ocean to the dust source than that from the Atlantic.
336 Given all of that, the Indian ocean SST used in this study was the summer average that was concurrent
337 with the dust season (Jun.–Jul.).

338 The relationship between DUCMASS and Niño-3 with Indian ocean SST signal removed also
339 experienced decadal variation. Figure 10 (a) showed that the correlation between Niño-3 and DUCMASS
340 was obviously reduced when the tropical western Indian ocean SSTA (TWISST) was removed from
341 Niño-3. As illustrated by Fig. 10 (b), during P1, TWISST weakened this correlation while no significant
342 contribution was observed during P2. Thus, it is hypothesized that TWISST weakened the impact of
343 ENSO on DUCMASS during P1. However, when the IOD (rather than TWISST) was considered, the
344 correlation between Niño-3 and DUCMASS kept the same when IOD was removed from Niño-3,
345 indicating that IOD exhibited no significant impact on the correlation between Niño-3 and DUCMASS.
346 Clark et al. (2000) showed that the SST in the central Indian Ocean exhibited stronger correlation with
347 the Indian precipitation than that in the Arabian Sea and northwest of Australia. Cherchi and Navarra
348 (2013) also pointed out that when the eastern and western poles of the IOD were considered separately,

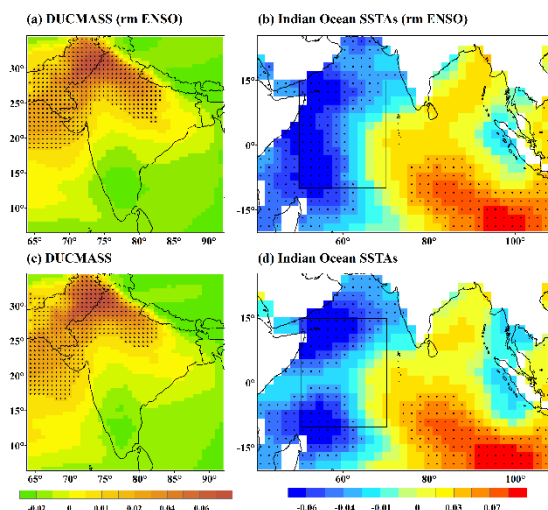
349 the western side exhibited the largest correlation. Thus, the TWISST was considered when exploring the
 350 effect of Indian ocean SSTA pattern on the DUCMASS–Niño-3 relationship.



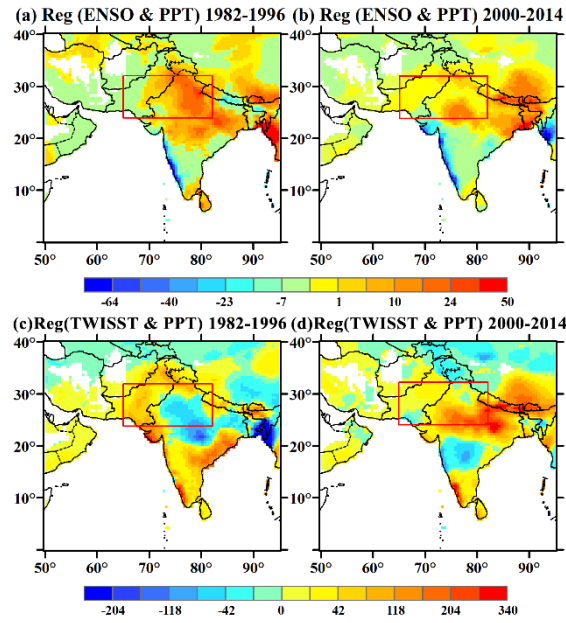
351
 352 **Figure 10: (a) The 15-year sliding correlation between DUCMASS and Niño-3 with and without TWISST-**
 353 **related signals removed; (b) Sliding contribution of TWISST to DUCMASS–Niño-3 relationship. The two red**
 354 **filled markers represented the 15-year window spanning from 1982 to 1996 and 2000 to 2014, respectively.**
 355 **The x-axis denotes the middle year of the period under analysis.**

356 The spatial coupling mode between DUCMASS and tropical Indian ocean SSTA showed that the
 357 cold tropical western Indian ocean and warm tropical eastern Indian ocean were coupled with higher
 358 DUCMASS over the northern and northwestern India. This pattern was not impacted by ENSO since the
 359 MCA results with ENSO-related signals removed were similar with that including the ENSO-related
 360 signals, as shown in Fig. 11. Figures 12–14 further illustrated the influence mechanism of Indian ocean
 361 SSTA pattern onto DUCMASS. Figure 12 showed that during P1, the regression coefficients between
 362 ENSO and PPT were opposite to the that between TWISST and PPT, while during P2, the regression
 363 coefficient between ENSO and DUCMASS as well as that between TWISST and DUCMASS were all
 364 positive. The similar changes were also seen when the effects of ENSO/TWISST on SoilM (Fig. 13), VP
 365 and wind field (Fig. 14) were considered. These illustrated the opposite effect of TWISST and ENSO on
 366 the key factors that influence the dust concentration, i.e., the local wind field and surface conditions. The
 367 above results further verified the inhibitory effect of Indian ocean SST pattern on the DUCMASS–Niño-
 368 3 relationship during P1, as well as the promotional effect during P2. In addition, to further elaborate the
 369 physical mechanisms of the interaction between ENSO and dust activities that was impacted by tropical
 370 western Indian ocean, the composite differences of the abovementioned climatic variables between El

371 Nino and La Nina years as well as that between positive TWITSST (TWITSST+) and negative TWITSST
 372 (TWITSST-) years were presented, as shown in Figs. S3-S5. Figures S3-S4 showed that the PPT and
 373 SoilM averaged from June to July in El Niño years exhibited positive anomalies, while that in La Niña
 374 years exhibited the reversed anomalies. The differences of PPT and SoilM between TWITSST+ and
 375 TWITSST- during P1 were negative, which were consistent with that between El Niño and La Niña
 376 conditions, while the differences during P2 were contrary to those during P1. Simultaneously, the
 377 differences of VP at 200hPa between TWITSST+ and TWITSST- also presented contrary change with
 378 those between El Niño and La Niña years during P1 and P2, as shown in Fig. S5. The mechanisms
 379 illustrated by the composite difference were analogous with the regression between dust activities and
 380 the climatic variables, both of which clarified the effect of TWITSST on the relationship between ENSO
 381 and dust activities over the northwestern South Asian dust source.



382
 383 **Figure 11: Spatial correlation between summer (Jun.–Jul.) tropical Indian ocean SSTA (TWISSTA) and**
 384 **DUCMASS of the first mode of the MCA analysis in 1982–2014. The first MCA mode of (a) the DUCMASS,**
 385 **and (b) the summer (Jun.–Jul.) tropical Indian ocean SSTA with ENSO-related signals removed. (c)–(d) As in**
 386 **(a)–(b), but for the original series including the ENSO signal. The black dots represent significance at ≥90 %**
 387 **confidence level.**

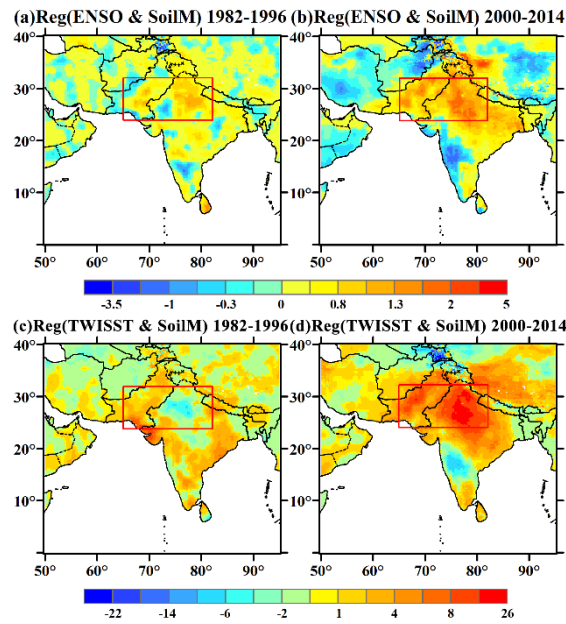


388

389

390

Figure 12: (a)–(b) Regression of ENSO with TWISST-related signals removed onto PPT in dust season (Jun.–Jul.); (c)–(d) Regression of TWISST with ENSO-related signals removed onto PPT in dust season (Jun.–Jul.).



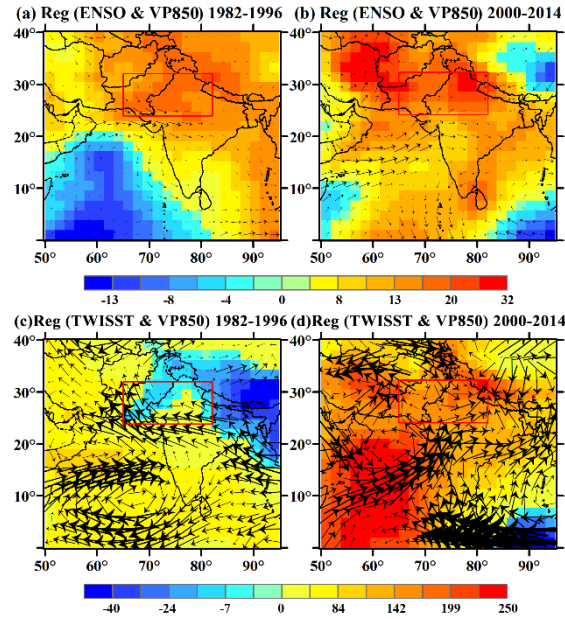
391

392

393

394

Figure 13: (a)–(b) Regression of ENSO with TWISST-related signals removed onto SoilM in dust season (Jun.–Jul.); (c)–(d) Regression of TWISST with ENSO-related signals removed onto SoilM in dust season (Jun.–Jul.).



395

396 **Figure 14: (a)–(b) Regression of ENSO with TWISST-related signals removed onto velocity potential at**
 397 **850hPa (VP850) and wind in dust season (Jun.–Jul.); (c)–(d) Regression of TWISST with ENSO-related**
 398 **signals removed onto velocity potential at 850hPa (VP850) and wind in dust season (Jun.–Jul.).**

399 3.2.3 Pacific Decadal Oscillation

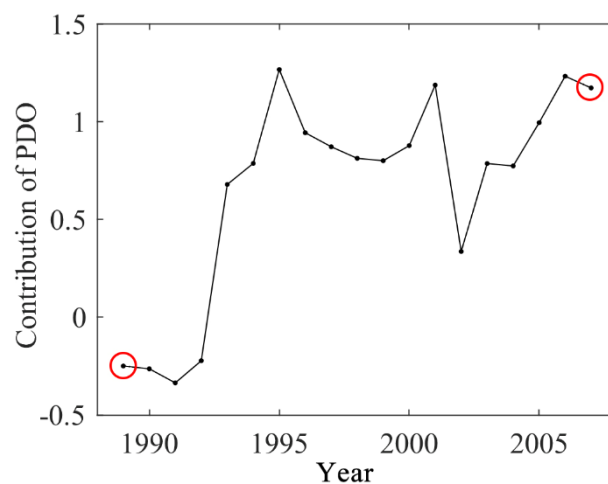
400 It is suggested that the PDO can influence the interannual variability of ISMR by enhancing the
 401 ENSO–ISMR relationship when ENSO and PDO were in-phase, while weakening the relationship when
 402 they were out of phase (Dong et al., 2018; Krishnamurthy and Krishnamurthy, 2014). However, it is
 403 unclear whether PDO is responsible for the shift of the DUCMASS–Niño-3 relationship. Table 2 listed
 404 the years with different phases of ENSO and PDO as well as years when ENSO and PDO are in (out of)
 405 phase separately. The correlation coefficient between ENSO and DUCMASS and significance level were
 406 also given. It demonstrated that the PDO significantly strengthened the correlation between ENSO and
 407 DUCMASS as the coefficient turned from -0.39 ($P>0.1$) when PDO and ENSO were out of phase to $-$
 408 0.69 ($P<0.01$) when they were in phase.

409 **Table 2: List of individual and combined wintertime ENSO–PDO years during 1982–2014.**

Events	Phase	
	Positive	Negative
ENSO	1983, 1987, 1988, 1991, 1993–1995,	1982, 1984–1986, 1989, 1996, 1997, 1998, 2003, 2005, 2007, 2010, 2015,
		1999–2001, 2006, 2008, 2009, 2011,

	2016, 2019	2012, 2014
PDO	1981–1988, 1996–1998, 2001, 2003– 2006, 2010, 2014–2019	1989, 1991, 1995, 1999, 2000, 2002, 2008, 2009, 2011, 2012
ENSO×PDO	1983, 1987–1989, 1998–2000, 2003, 2005, 2008–2012	1982, 1984–1986, 1991, 1995–1997, 2001, 2006, 2014
R (Niño-3 & DUCMASS)	–0.69 (P<0.01)	–0.39 (P>0.1)

410 Table 2 revealed that P2 includes most of years (8 out of 14) when ENSO and PDO were in-phase,
 411 i.e., 2000, 2003, 2005, and 2008–2012, while most of the out-of-phase years (8 out of 11) appeared in
 412 P1, i.e., 1982, 1984–1986, 1991, 1995, 1996, and 1997. Simultaneously, the winter Niño-3 exhibited
 413 lower correlation with DUCMASS in P1 when most of ENSO years were accompanied with anti-phase
 414 PDO. In addition, the quantitative contribution of PDO shown in Fig. 15 further confirmed that the PDO
 415 strengthened the impact of ENSO on DUCMASS in P2 while the contribution was close to 0.0 in P1. All
 416 those demonstrated that the phase shift of PDO plays an important role in modulating the revolution of
 417 DUCMASS–Niño-3 relationship.

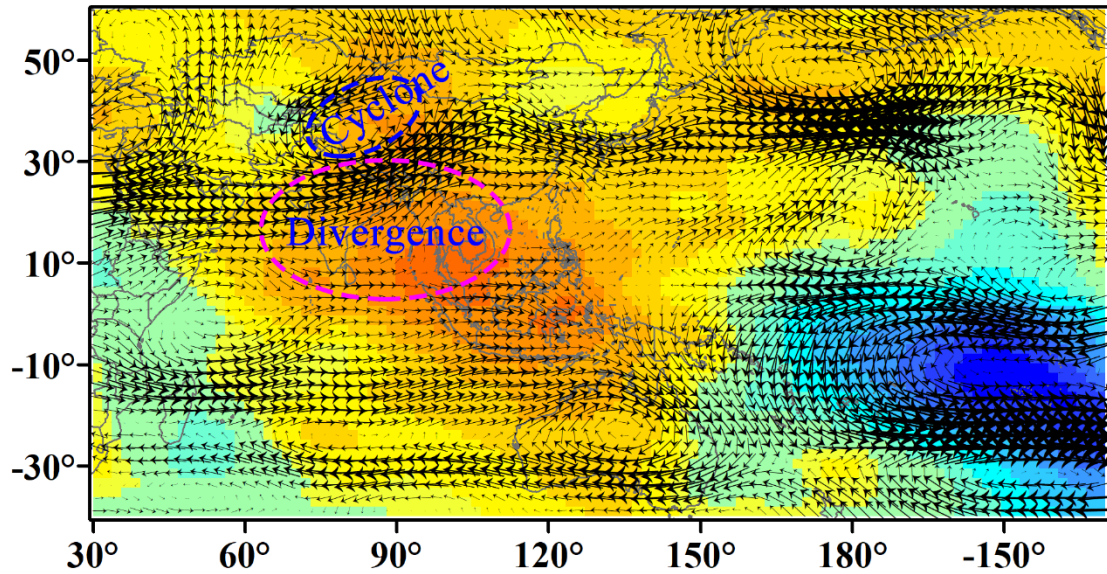


418
 419 **Figure 15: Sliding contribution of PDO to DUCMASS–Niño-3 relationship. The two circles represented the**
 420 **15-year window spanning from 1982 to 1996 and 2000 to 2014, respectively.**

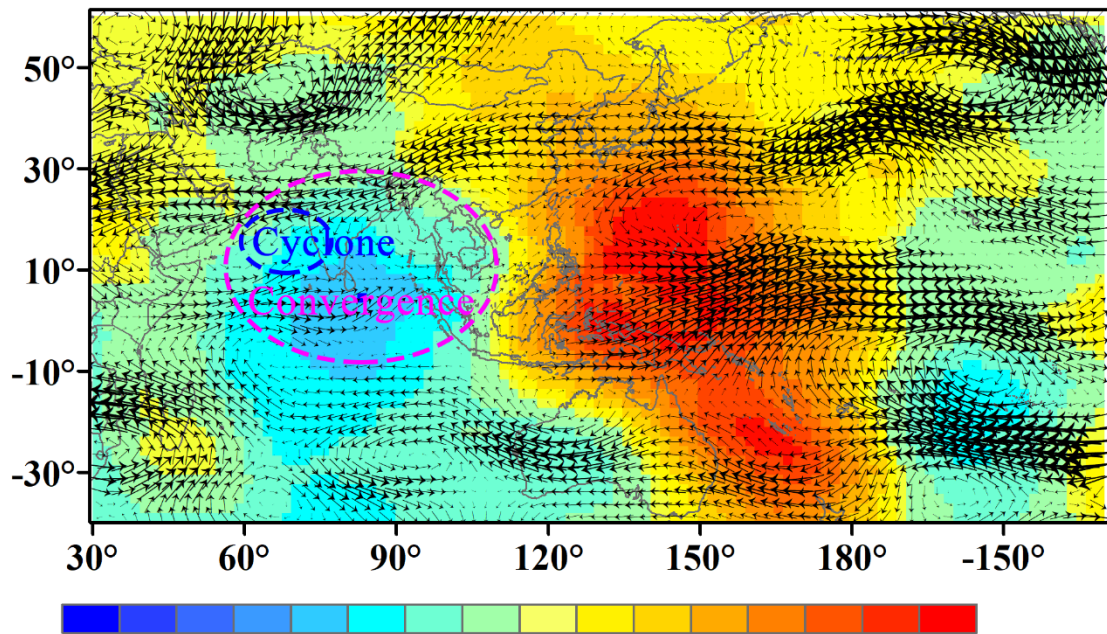
421 Figure 16 revealed the influence mechanism of PDO onto DUCMASS. During P1, the 200hPa
 422 velocity potential in the positive PDO years exhibited a decrease (convergence) over the eastern tropical
 423 Pacific and an increase (divergence) over the tropical Indian Ocean and Indian subcontinent (Fig. 16 (a)).
 424 The upper-level divergence over India and the adjacent seas corresponded to the anomalous ascending

425 motion, which promoted ISMR and consequently suppressed the dust storms over South Asia.
426 Meanwhile, an anomalous cyclone developed to the north of India due to the enhanced convection. The
427 westerlies on the southern flank of the cyclonic anomaly transported wet air from the Arabian Sea to the
428 northwest of India (Huang et al., 2020), which further inhibited dust emissions. While in the negative
429 PDO years during P2, the 200hPa velocity potential exhibited a decrease (convergence) over India,
430 corresponding to an anomalous descending motion, as shown in Fig. 16 (b). This descending flow
431 suppressed the Indian monsoon convection and rainfall, which consequently enhanced dust emissions.
432 Similarly, an anomalous cyclone developed over the south of India. The easterlies on the northern flank
433 of the cyclonic anomaly advected relatively drier air from the Eurasian continent to the northern India
434 (Parker et al., 2016), which favored dust emissions. The difference of flow movements and their effects
435 on dust activities between positive and negative PDO years was consistent with that between El Niño
436 and La Niña years, which further proved that PDO could significantly strengthen the effect of ENSO on
437 DUCMASS when it was in phase with ENSO.

(a) Reg of VP & UV at 200hPa onto PDO in 1982-1996



(b) Reg of VP & UV at 200hPa onto PDO in 2000-2014



-125.2 -90.8 -53.2 -16.7 6.5 29.4 57.5 83.7 $\times 10^4 \text{ m}^2/\text{s}$

438

439 **Figure 16: (a) Regression of summer (Jun.–Jul.) velocity potential at 200hPa onto previous winter PDO**
440 **(averaged from Nov. to Jan.) overlaid with the average of summer wind in positive PDO years during 1982–**
441 **1996; (b) Regression of summer velocity potential at 200hPa onto previous winter PDO overlaid with the**
442 **average of summer wind in negative PDO years during 2000–2014.**

443 **4 Discussion**

444 **4.1 Response of Atlantic SSTA pattern to CT/EM ENSO**

445 It was reported that the interdecadal shift of tropical Atlantic SSTA pattern was a response to the

446 multi-year ENSO events (Tokinaga et al., 2019). The multi-year ENSO event, namely continuing ENSO
 447 (CT ENSO), was a situation where the summer ENSO SSTA continued from the preceding year. Another
 448 type of ENSO, which was called as emerging ENSO (EM ENSO), was characterized as late Atlantic
 449 SSTA response that started from June. The CT ENSO primarily dominated during P1, while P2 was
 450 dominated by EM ENSO (Yang and Huang, 2021). The impact of the two types of ENSO on the shift of
 451 the DUCMASS–Niño-3 relationship were examined. Table 3 showed that ASGI was significantly
 452 correlated with Niño-3 in the CT ENSO years, which was not observed in the EM ENSO years.
 453 Simultaneously, DUCMASS was significantly related to Niño-3 only in the EM ENSO years. The
 454 composite correlation difference between CT and EM ENSOs was consistent with that between the
 455 period of P1 and P2, indicating that the shift of Atlantic SSTA pattern, which was prominently modulated
 456 by the type of ENSO, plays an important role in modulating the DUCMASS–Niño-3 relationship.

457 **Table 3: Correlation between ASGI and Niño-3 as well as DUCMASS in two different phases (* and *****
 458 **indicate the correlations that are significant on a 0.1 and 0.01 level, respectively).**

R	CT ENSO	EM ENSO	P1	P2
ASGI & Niño-3	0.78 (***)	0.19	0.73 (***)	0.46 (*)
DUCMASS & Niño-3	-0.60 (*)	-0.75 (***)	-0.51 (*)	-0.67 (***)

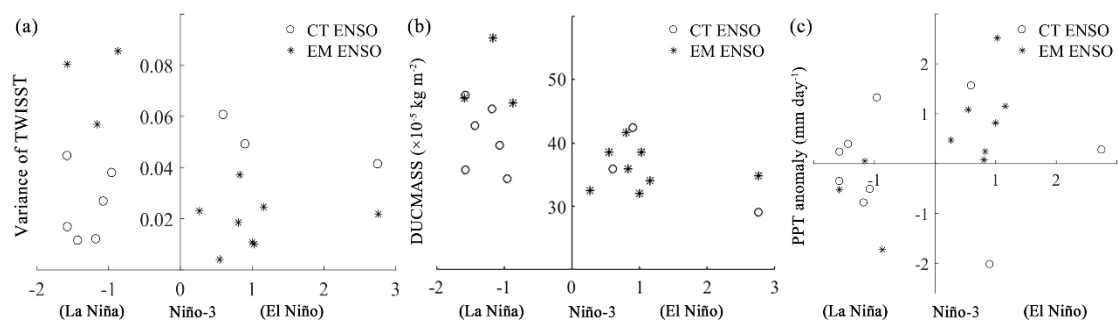
459

460 4.2 Response of Indian ocean SSTA pattern to CT/EM ENSO

461 As discussed in Sect. 3.2.2, ENSO can affect the Indian Ocean SST and the Indian Ocean variability
 462 can also modulate the ENSO variability (Wu and Kirtman, 2004; Yu et al., 2002; Kug et al., 2005). It is
 463 known that during CT ENSO years, the ENSO event in summer primarily starts from the preceding
 464 winter, while in EM ENSO years, the ENSO event mainly emerges in late spring (Yang and Huang, 2021).
 465 Correspondingly, the associated Indian Ocean SST oscillation also varies in these two different ENSO
 466 years. In order to explore whether the different types of ENSO impacted the DUCMASS over the
 467 northwestern South Asia through adjusting the duration of the temperature anomaly, we compared the
 468 SST and the variance of the monthly SSTA from (–1) Sep. to (0) May over the tropical western Indian
 469 ocean (TWISSTA).

470 Figure 17 (a) showed that the variances in the EM La Niña years were generally larger than that in

471 the CT La Niña years, while the variances in the EM El Niño years were generally smaller than that in
 472 the CT El Niño years. Concurrently, the difference of DUCMASS in El Niño and La Niña years was
 473 obvious in the EM ENSO period with higher values appeared in La Niña years (Fig. 17 (b)). However,
 474 in the CT ENSO period, no significant difference was observed between El Niño and La Niña years.
 475 Therefore, it is hypothesized that the EM ENSO conditions, which was associated with higher TWISST
 476 variance, were more favorable to trigger the variation of DUCMASS. Yang and Huang (2021) reported
 477 that P1 was primarily dominated by CT ENSOs while EM ENSOs primarily controlled during P2.
 478 Combined with abovementioned hypothesis, the correlation between DUCMASS and Niño-3 should be
 479 higher in P2, which was consistent with the interdecadal change of this relationship. Figure 17 (c) further
 480 revealed the influence mechanism of TWISSTA onto DUCMASS. It showed that compared to CT ENSO
 481 type, the difference of PPT between El Niño and La Niña years was more significant in the EM ENSO
 482 years, in addition, the PPT in La Niña years (with high TWISSTA variance) was lower than that in El
 483 Niño years (with low TWISSTA variance), which was contrary to the difference of DUCMASS between
 484 those two types of ENSO years. While when other atmospheric factors were considered, such as land
 485 cover and winds at multi-layers, no similar change was observed. This indicated that the Indian Ocean
 486 SSTA, which was also remarkably modulated by the type of ENSO, impacted DUCMASS by adjusting
 487 the PPT and further influenced the relationship between ENSO and DUCMASS.



488
 489 **Figure 17: Scatter diagram between (a) variance of the monthly TWISSTA from (-1) Sep. to (0) May, (b)**
 490 **DUCMASS, and (c) PPT anomaly and Niño-3 index separately for continuing (CT) and emerging (EM) ENSO.**

491 4.3 Uncertainty in analyzing the contribution of the influence factors

492 The contributions of those abovementioned factors to the interdecadal shift of ENSO-DUCMASS
 493 relationship were analyzed based on the linear regression model. However, the linear regression model
 494 would definitely bring uncertainty to the results (Guo et al., 2017) and may not be sufficient to verify the

495 cause and effect. Thus, the numerical models are suggested for future research to quantify the
496 contribution of those factors to the shift of ENSO–DUCMASS relationship. However, before such
497 quantitative study the regression analysis is indispensable to identify the possible driving factors. In this
498 context, it is undeniable that this study provides new sights to the dust storm-related numerical simulation
499 by taking account of the teleconnections and their influence mechanisms.

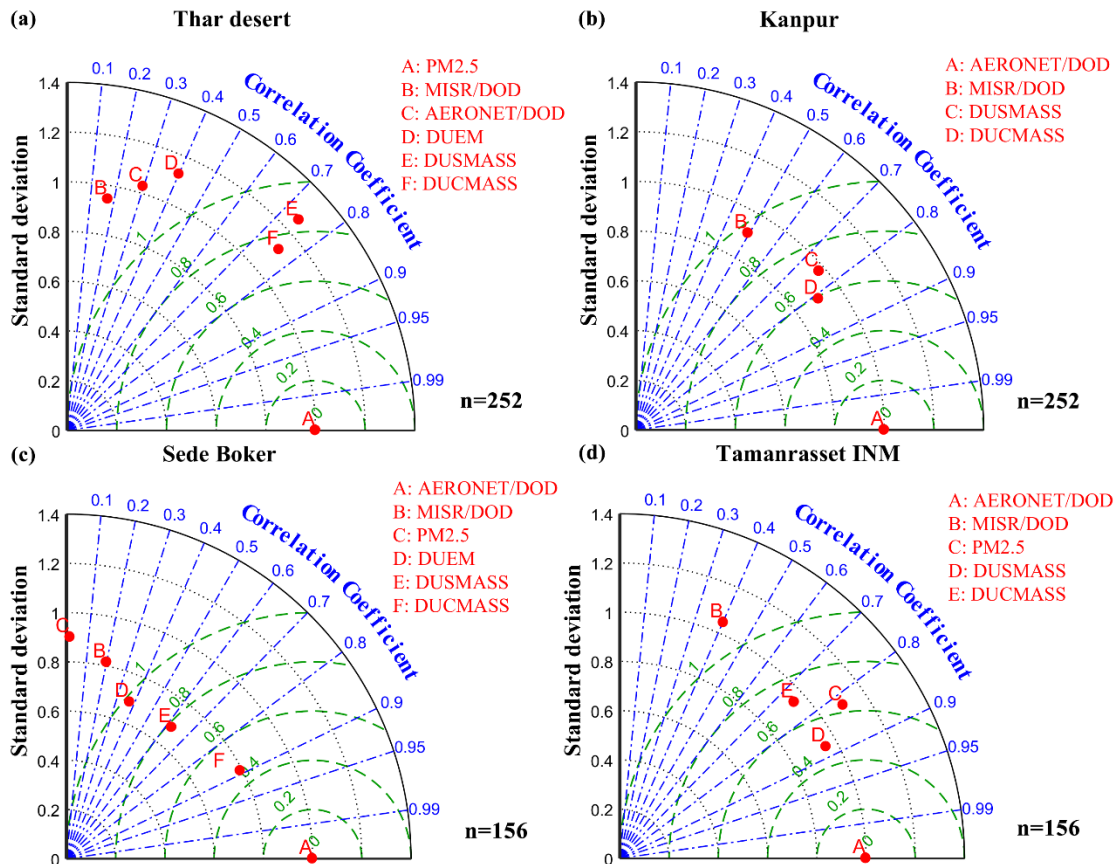
500 In addition, while analyzing the effects of different types of ENSO event, we compared the variance
501 of TWISST and DUCMASS under the two types of ENSO periods, as shown in Fig. 17. It showed that
502 only eight EM ENSO years were identified and the number of PDO years that were in or out of phase
503 with ENSO were also insufficient. The statistical results acquired from the insufficient number of
504 samples could also be explained by the random events (Pallikari, 2004). In order to verify this conclusion,
505 we calculated the interannual correlation between the variance of TWISST and DUCMASS from 1982
506 to 2014. Even so, the significant interannual correlation does not guarantee the significant link between
507 different types of ENSO. Therefore, longer time series with valid samples (i.e., CT/EM ENSO and PDO
508 years) are needed to further validate the influence of ENSO types on the ENSO–DUCMASS relationship
509 in the future. Alternatively, using numerical model to simulate the teleconnection pattern of ENSO over
510 South Asia under different types of ENSO is also favorable.

511 Except for the large-scale atmospheric circulation, the anthropogenic land-use management could
512 also play an important role in the interdecadal variability of ENSO–DUCMASS relationship (Kumar et
513 al., 1999), which should be considered in the future researches.

514 The dust activities analyzed in this study were from the dust season, i.e., Jun.–Jul., which were part
515 of monsoon season (Jun.–Sep.) (Babu et al., 2013), however, the dust activities during pre-monsoon
516 season (Mar.–May or Apr.–May) were also a hot topic (Babu et al., 2013; Lakshmi et al., 2017, 2019).
517 Therefore, we analyzed the interdecadal change of the ENSO impact on DUCMASS during dust season
518 (Jun.–Jul.) and pre-monsoon (Mar.–May or Apr.–May) separately, to find that the significant interdecadal
519 change occurred only when the DUCMASS during dust season was considered. As for that during pre-
520 monsoon season, there should be some other factors that influenced its interdecadal change, which will
521 be discussed in the future study.

522 4.4 Precision validation of MERRA-2 dust concentration dataset

523 It is known that the nonspherical aerosol optical depth retrieved from satellite, concentration of
524 PM_{2.5}/PM₁₀ and coarse mode aerosol optical depth acquired from observation stations represent
525 extinction characteristics of dust aerosols in the whole atmospheric column, thus they can be used to
526 validate the dust column concentration datasets but not appropriate for the validation of dust emission,
527 which reflect the dust loading lifted from ground. The dust dataset used in this study was the dust column
528 concentration “Dust Column Mass Density-PM_{2.5}”, thus the PM_{2.5}, coarse mode aerosol optical depth
529 acquired from AERONET (AERONET/DOD), and nonspherical aerosol optical depth retrieved from
530 MISR (MISR/DOD) was utilized to validate the precision of DUCMASS dataset. The time coverage and
531 continuity of satellite and observation-based products lagged behind the MERRA-2 datasets, thus only
532 several stations over the dust belt with relatively longer time series were chosen. They were Kanpur (26.5°
533 N, 80.2° E. Time span: 2001–2021), Sede Boker (30.9° N, 34.8° E. Time span: 2007–2019), and
534 Tamanrasset INM (22.8° N, 5.5° E. Time span: 2007–2019). The MISR/DOD, PM_{2.5}, and dust variables
535 from MERRA-2 were the regional average within 1° of the corresponding station. No dust emission was
536 observed over the Kanpur and Tamanrasset INM station. Besides, the datasets over the study area
537 (represented by Thar desert in Fig. 18 (a)) were also accounted and the AERONET/DOD was obtained
538 from the nearest Kanpur station. For the study area, PM_{2.5} was chosen as the reference dataset (A) because
539 the study area was not overlapped with the Kanpur station, while AERONET/DOD was chosen as the
540 reference data for other stations.



541

542

543

544

545

546

Figure 18: Normalized Taylor diagrams showing (a) difference between dust variables acquired from MISR, AERONET, MERRA2 datasets and that acquired from PM_{2.5} dataset, and (b–d) difference between dust variables from MISR, PM_{2.5}, MERRA2 datasets and that acquired from AERONET dataset. The normalized standard deviation is on the radial axis (black contours); correlation coefficient is on the angular axis (blue contours); and green dashed lines indicate centered RMSE. N indicates the sample size.

547

Figure 18 (a) compared the precision of MISR/DOD, AERONET/DOD, dust emission (DUEM),

548

surface dust mass concentration (DUSMASS), and DUCMASS with that of PM_{2.5}, it showed that no

549

significant correlation was observed between AERONET/DOD and PM_{2.5} because this study area did not

550

coincide with the Kanpur station. However, the correlations between PM_{2.5} and DUSMASS as well as

551

DUCMASS were significant ($R > 0.7$, $RMSE < 0.9$) and stronger than that between PM_{2.5} and DUEM.

552

Figure 18 (b) showed the precision of MISR/DOD, DUSMASS, and DUCMASS compared with

553

AERONET/DOD over the Kanpur station. The results indicated that both DUSMASS and DUCMASS

554

were significantly correlated with AERONET/DOD ($R > 0.7$, $RMSE < 0.8$). In addition, the comparison

555

results over the other two stations also indicated that DUSMASS and DUCMASS were significantly

556

correlated with AERONET/DOD, while the relationship between DUEM and AERONET/DOD was

557

weak, as shown in Figs. 18 (c)–(d). The above results demonstrated that the DUCMASS from MERRA-

558

2 was strongly consistent with MISR/DOD, AERONET/DOD, and PM_{2.5}, indicating that the DUCMASS

559 datasets used in this study were relatively reliable for researches about dust.

560 **5 Conclusions**

561 In the study, we revealed the interdecadal change of the ENSO impact on DUCMASS over the
562 northwestern South Asia from 1982 to 2014, and further investigated the factors contributing to the shifts
563 of the responses of DUCMASS to the wintertime ENSO. It was found that the ENSO–DUCMASS
564 relationship shifted from weak negative relation during 1982–1996 to significant negative correlation
565 during 2000–2014. The change of Atlantic and Indian ocean SSTA pattern weakened the impact of
566 wintertime ENSO on dust activities over the northwestern South Asia during 1982–1996, while PDO
567 tended to strengthen ENSO’s effect on dust activities when it was in phase with ENSO. Both the Atlantic
568 and Indian Ocean SSTA patterns were modulated by the duration of ENSO events (i.e., continuing and
569 emerging ENSO). The current results are based solely on the linear regression, and further studies
570 integrating numerical models and longer time series are needed to validate the results. Nevertheless, this
571 study indeed found multiple large-scale factors that could impact the interdecadal interaction between
572 ENSO and dust activities over the northwestern South Asia. Given that it is possible to forecast the
573 change of some large-scale atmospheric circulation patterns, the results of this study could provide new
574 insight to the prediction of dust storm trend in the near future based on the variability of ENSO–
575 DUCMASS relationship.

576 **Data availability**

577 The data can be downloaded for free from the corresponding website which were listed in the text.

578 **Author contribution**

579 L.S. designed the study, performed the analysis with feedback from J.Z. and F.Y., and wrote the
580 paper that was reviewed by J.Z., F.Y., D.Z., J.W., X.M., and Y.L.. All the authors discussed the results.

581 **Competing interests**

582 The authors declare that they have no conflict of interest.

583 **Acknowledgments**

584 The authors would like to thank the Modern-Era Retrospective Analysis for Research and
585 Applications, version 2 (MERRA-2) for providing the surface dust mass concentration, wind speed and
586 planetary boundary layer height, the National Oceanic and Atmospheric Administration (NOAA) for
587 providing the SST, the Hadley Centre Climate Research Unit for the land-surface temperature and
588 precipitation, the National Aeronautics and Space Administration (NASA) for the NDVI, and the Climate
589 Predict Center of National Oceanic and Atmospheric Administration (NOAA/CPC) for the large-scale
590 climate indices.

591 This work was supported by the Strategic Priority Research Program of the Chinese Academy of
592 Sciences-A (No. XDA19030402) and the National Natural Science Foundation of China (No. 42071425).

593 **References**

- 594 Abish, B. and Mohanakumar, K.: Absorbing aerosol variability over the Indian subcontinent and its
595 increasing dependence on ENSO, *Glob. Planet. Change*, 106, 13–19,
596 <https://doi.org/10.1016/j.gloplacha.2013.02.007>, 2013.
- 597 Ashok, K., Behera, S. K., Rao, S. A., Weng, H., and Yamagata, T.: El Nino Modoki and its possible
598 teleconnection, *J. Geophys. Res.*, 112, C11007, 2007.
- 599 Augustyn, A., Zeidan, A., Zelazko, A., Eldridge, A., McKenna, A., Tikkanen, A., Gadzikowski, A.,
600 Schreiber, B. A., Duignan, B., Mahajan, D., Promeet, D., Goldstein, E., and Rodriguez, E.: Thar
601 Desert, *Encycl. Br.*, 2019.
- 602 Avila, A.: The chemical composition of dust transported in red rains—its contribution to the
603 biogeochemical cycle of a holm oak forest in Catalonia (Spain), *Atmos. Environ.*, 32, 179–191, 1998.
- 604 Babu, S. S., Manoj, M. R., Moorthy, K. K., Gogoi, M. M., Nair, V. S., Kompalli, S. K., Satheesh, S. K.,
605 Niranjana, K., Ramagopal, K., Bhuyan, P. K., and Singh, D.: Trends in aerosol optical depth over
606 Indian region: Potential causes and impact indicators, *J. Geophys. Res. Atmos.*, 118, 11,794–11,806,
607 <https://doi.org/10.1002/2013JD020507>, 2013.
- 608 Banerjee, P. and Kumar, S. P.: ENSO modulation of interannual variability of dust aerosols over the
609 northwest Indian Ocean, *J. Clim.*, 29, 1391–1415, <https://doi.org/10.1175/JCLI-D-15-0039.1>, 2016.

610 Banerjee, P., Satheesh, S. K., Moorthy, K. K., Nanjundiah, R. S., and Nair, V. S.: Long-range transport
611 of mineral dust to the northeast Indian Ocean: Regional versus remote sources and the implications,
612 *J. Clim.*, 32, 1525–1549, <https://doi.org/10.1175/JCLI-D-18-0403.1>, 2019.

613 Behrooz, R. D., Esmaili-Sari, A., Bahramifar, N., and Kaskaoutis, D. G.: Analysis of the TSP, PM10
614 concentrations and water-soluble ionic species in airborne samples over Sistan, Iran during the
615 summer dusty period, *Atmos. Pollut. Res.*, 8, 403–417, 2017.

616 Bollasina, M. A., Ming, Y., and Ramaswamy, V.: Anthropogenic aerosols and the weakening of the
617 south asian summer monsoon, *Science* (80-.), 334, 502–505,
618 <https://doi.org/10.1126/science.1204994>, 2011.

619 Bozlaker, A., Prospero, J. M., Fraser, M. P., and Chellam, S.: Quantifying the contribution of long-range
620 saharan dust transport on particulate matter concentrations in Houston, Texas, using detailed
621 elemental analysis, *Environ. Sci. Technol.*, 47, 10179–10187, <https://doi.org/10.1021/es4015663>,
622 2013.

623 Buchard, V., Randles, C. A., da Silva, A. M., Darmenov, A., Colarco, P. R., Govindaraju, R., Ferrare,
624 R., Hair, J., Beyersdorf, A. J., Ziemba, L. D., and Yu, H.: The MERRA-2 aerosol reanalysis, 1980
625 onward. Part II: Evaluation and case studies, *J. Clim.*, 30, 6851–6872, [https://doi.org/10.1175/JCLI-](https://doi.org/10.1175/JCLI-D-16-0613.1)
626 [D-16-0613.1](https://doi.org/10.1175/JCLI-D-16-0613.1), 2017.

627 Cai, W., Borlace, S., Lengaigne, M., Van Rensch, P., Collins, M., Vecchi, G., Timmermann, A., Santoso,
628 A., Mcphaden, M. J., Wu, L., England, M. H., Wang, G., Guilyardi, E., and Jin, F. F.: Increasing
629 frequency of extreme El Niño events due to greenhouse warming, *Nat. Clim. Chang.*, 4, 111–116,
630 <https://doi.org/10.1038/nclimate2100>, 2014.

631 Chauhan, S. S.: Desertification control and management of land degradation in the Thar desert of India,
632 *Environmentalist*, 23, 219–227, <https://doi.org/10.1023/B:ENVR.0000017366.67642.79>, 2003.

633 Chen, Y.-S., Sheen, P.-C., Chen, E.-R., Liu, Y.-K., Wu, T.-N., and Yang, C.-Y.: Effects of Asian dust
634 storm events on daily mortality in Taipei, Taiwan., *Environ. Res.*, 95, 151–155,
635 <https://doi.org/10.1016/j.envres.2003.08.008>, 2004.

636 Cherchi, A. and Navarra, A.: Influence of ENSO and of the Indian Ocean Dipole on the Indian summer
637 monsoon variability, *Clim. Dyn.*, 41, 81–103, <https://doi.org/10.1007/s00382-012-1602-y>, 2013.

638 Clark, C. O., Cole, J. E., and Webster, P. J.: Indian Ocean SST and Indian summer rainfall: Predictive
639 relationships and their decadal variability, *J. Clim.*, 13, 2503–2519, [https://doi.org/10.1175/1520-0442\(2000\)013<2503:IOSAIS>2.0.CO;2](https://doi.org/10.1175/1520-0442(2000)013<2503:IOSAIS>2.0.CO;2), 2000.

641 Dong, B., Dai, A., Vuille, M., and Timm, O. E.: Asymmetric modulation of ENSO teleconnections by
642 the interdecadal Pacific oscillation, *J. Clim.*, 31, 7337–7361, <https://doi.org/10.1175/JCLI-D-17-0663.1>, 2018.

644 Du, Y., Xie, S. P., Huang, G., and Hu, K.: Role of air-sea interaction in the long persistence of El Niño-
645 induced north Indian Ocean warming, *J. Clim.*, 22, 2023–2038, <https://doi.org/10.1175/2008JCLI2590.1>, 2009.

647 Easterling, D. R. and Wehner, M. F.: Is the climate warming or cooling?, *Geophys. Res. Lett.*, 36, 4–6,
648 <https://doi.org/10.1029/2009GL037810>, 2009.

649 Erel, Y., Dayan, U., Rabi, R., Rudich, Y., and Stein, M.: Trans boundary transport of pollutants by
650 atmospheric mineral dust, *Environ. Sci. Technol.*, 40, 2996–3005, <https://doi.org/10.1021/es051502l>,
651 2006.

652 Fyfe, J. C., Merryfield, W. J., Kharin, V., Boer, G. J., Lee, W. S., and Von Salzen, K.: Skillful predictions
653 of decadal trends in global mean surface temperature, *Geophys. Res. Lett.*, 38, 1–5,
654 <https://doi.org/10.1029/2011GL049508>, 2011.

655 Fyfe, J. C., Gillett, N. P., and Zwiers, F. W.: Overestimated global warming over the past 20 years, *Nat.*
656 *Clim. Chang.*, 3, 767–769, <https://doi.org/10.1038/nclimate1972>, 2013.

657 Gelaro, R., McCarty, W., Suárez, M. J., Todling, R., Molod, A., Takacs, L., Randles, C. A., Darmenov,
658 A., Bosilovich, M. G., Reichle, R., Wargan, K., Coy, L., Cullather, R., Draper, C., Akella, S., Buchard,
659 V., Conaty, A., da Silva, A. M., Gu, W., Kim, G. K., Koster, R., Lucchesi, R., Merkova, D., Nielsen,
660 J. E., Partyka, G., Pawson, S., Putman, W., Rienecker, M., Schubert, S. D., Sienkiewicz, M., and
661 Zhao, B.: The modern-era retrospective analysis for research and applications, version 2 (MERRA-
662 2), *J. Clim.*, 30, 5419–5454, <https://doi.org/10.1175/JCLI-D-16-0758.1>, 2017.

663 Graham, N. E.: Decadal-scale climate variability in the tropical and North Pacific during the 1970s and
664 1980s: observations and model results, *Clim. Dyn.*, 10, 135–162,
665 <https://doi.org/10.1007/BF00210626>, 1994.

666 Guo, H., Wang, X., and Gao, Z.: Uncertain linear regression model and its application, *J. Intell. Manuf.*,
667 28, 559–564, <https://doi.org/10.1007/s10845-014-1022-4>, 2017.

668 Hansen, J. E., Sato, M., and Ruedy, R.: Radiative forcing and climate response, *J. Geophys. Res. Atmos.*,
669 102, 6831–6864, 1997.

670 He, L., Lin, A., Chen, X., Zhou, H., Zhou, Z., and He, P.: Assessment of MERRA-2 Surface PM_{2.5} over
671 the Yangtze River Basin: Ground-based verification, spatiotemporal distribution and meteorological
672 dependence, *Remote Sens.*, 11, 460, <https://doi.org/10.3390/rs11040460>, 2019.

673 He, S. and Wang, H.: Oscillating relationship between the East Asian Winter Monsoon and ENSO, *J.*
674 *Clim.*, 26, 9819–9838, <https://doi.org/10.1175/JCLI-D-13-00174.1>, 2013.

675 Hirahara, S., Ishii, M., and Fukuda, Y.: Centennial-scale sea surface temperature analysis and its
676 uncertainty, *J. Clim.*, 27, 57–75, <https://doi.org/10.1175/JCLI-D-12-00837.1>, 2014.

677 Hu, S. and Fedorov, A. V.: The extreme El Niño of 2015–2016 and the end of global warming hiatus,
678 *Geophys. Res. Lett.*, 44, 3816–3824, <https://doi.org/10.1002/2017GL072908>, 2017.

679 Huang, J., Wang, T., Wang, W., Li, Z., and Yan, H.: Climate effects of dust aerosols over East Asian
680 arid and semiarid regions, *J. Geophys. Res. Atmos.*, 119, 11398–11416,
681 <https://doi.org/10.1038/175238c0>, 2014.

682 Huang, X., Zhou, T., Turner, A., Dai, A., Chen, X., Clark, R., Jiang, J., Man, W., Murphy, J., Rostron,
683 J., Wu, B., Zhang, L., Zhang, W., and Zou, L.: The recent decline and recovery of Indian summer
684 monsoon rainfall: Relative roles of external forcing and internal variability, *J. Clim.*, 33, 5035–5060,
685 <https://doi.org/10.1175/JCLI-D-19-0833.1>, 2020.

686 Jin, Q. and Wang, C.: The greening of Northwest Indian subcontinent and reduction of dust abundance
687 resulting from Indian summer monsoon revival, *Sci. Rep.*, 8, 1–9, [https://doi.org/10.1038/s41598-](https://doi.org/10.1038/s41598-018-23055-5)
688 018-23055-5, 2018.

689 Jin, Q., Wei, J., Pu, B., Yang, Z. L., and Parajuli, S. P.: High Summertime Aerosol Loadings Over the
690 Arabian Sea and Their Transport Pathways, *J. Geophys. Res. Atmos.*, 123, 10,568-10,590,
691 <https://doi.org/10.1029/2018JD028588>, 2018.

692 Jin, Q., Wei, J., Lau, W. K. M., Pu, B., and Wang, C.: Interactions of Asian mineral dust with Indian
693 summer monsoon: Recent advances and challenges, *Earth-Science Rev.*, 215, 103562,

694 <https://doi.org/10.1016/j.earscirev.2021.103562>, 2021.

695 Kaiser, J. and Granmar, M.: Mounting Evidence Indicts Fine-Particle Pollution, *Science* (80-.), 307,
696 1858–1861, 2005.

697 Kinter, I. L., Miyakoda, K., and Yang, S.: Recent change in the connection from the Asian monsoon to
698 ENSO, *J. Clim.*, 15, 1203–1215, [https://doi.org/10.1175/1520-0442\(2002\)015<1203:RCITCF>2.0.CO;2](https://doi.org/10.1175/1520-0442(2002)015<1203:RCITCF>2.0.CO;2), 2002.

700 Kosaka, Y. and Xie, S. P.: Recent global-warming hiatus tied to equatorial Pacific surface cooling, *Nature*,
701 501, 403–407, <https://doi.org/10.1038/nature12534>, 2013.

702 Krishnamurthy, L. and Krishnamurthy, V.: Influence of PDO on South Asian summer monsoon and
703 monsoon-ENSO relation, *Clim. Dyn.*, 42, 2397–2410, <https://doi.org/10.1007/s00382-013-1856-z>,
704 2014.

705 Krishnamurthy, V. and Kirtman, B. P.: Variability of the Indian Ocean: Relation to monsoon and ENSO,
706 *Q. J. R. Meteorol. Soc.*, 129, 1623–1646, <https://doi.org/10.1256/qj.01.166>, 2003.

707 Kucharski, F., Bracco, A., Yoo, J. H., and Molteni, F.: Low-frequency variability of the Indian monsoon-
708 ENSO relationship and the tropical Atlantic: The “weakening” of the 1980s and 1990s, *J. Clim.*, 20,
709 4255–4266, <https://doi.org/10.1175/JCLI4254.1>, 2007.

710 Kug, J. S., An, S. Il, Jin, F. F., and Kang, I. S.: Preconditions for El Niño and La Niña onsets and their
711 relation to the Indian Ocean, *Geophys. Res. Lett.*, 32, 1–5, <https://doi.org/10.1029/2004GL021674>,
712 2005.

713 Kumar, K. K., Rajagopalan, B., and Cane, M. A.: On the weakening relationship between the indian
714 monsoon and ENSO, *Science* (80-.), 284, 2156–2159,
715 <https://doi.org/10.1126/science.284.5423.2156>, 1999.

716 Lakshmi, N. B., Nair, V. S., and Suresh Babu, S.: Vertical structure of aerosols and mineral dust over
717 the Bay of Bengal from multisatellite observations, *J. Geophys. Res. Atmos.*, 122, 12,845–12,861,
718 <https://doi.org/10.1002/2017JD027643>, 2017.

719 Lakshmi, N. B., Babu, S. S., and Nair, V. S.: Recent Regime Shifts in Mineral Dust Trends over South
720 Asia from Long-Term CALIPSO Observations, *IEEE Trans. Geosci. Remote Sens.*, 57, 4485–4489,
721 <https://doi.org/10.1109/TGRS.2019.2891338>, 2019.

722 Lee, Y. G., Kim, J., Ho, C. H., An, S. Il, Cho, H. K., Mao, R., Tian, B., Wu, D., Lee, J. N., Kalashnikova,
723 O., Choi, Y., and Yeh, S. W.: The effects of ENSO under negative AO phase on spring dust activity
724 over northern China: An observational investigation, *Int. J. Climatol.*, 35, 935–947,
725 <https://doi.org/10.1002/joc.4028>, 2015.

726 Li, T., Zhang, Y., Lu, E., and Wang, D.: Relative role of dynamic and thermodynamic processes in the
727 development of the Indian Ocean dipole: An OGCM diagnosis, *Geophys. Res. Lett.*, 29,
728 <https://doi.org/10.1029/2002GL015789>, 2002.

729 Liu, J., Wu, D., Liu, G., Mao, R., Chen, S., Ji, M., Fu, P., Sun, Y., Pan, X., Jin, H., Zhou, Y., and Wang,
730 X.: Impact of Arctic amplification on declining spring dust events in East Asia, *Clim. Dyn.*, 54, 1913–
731 1935, <https://doi.org/10.1007/s00382-019-05094-4>, 2020.

732 Mahowald, N., Albani, S., Kok, J. F., Engelstaeder, S., Scanza, R., Ward, D. S., and Flanner, M. G.: The
733 size distribution of desert dust aerosols and its impact on the Earth system, *Aeolian Res.*, 15, 53–71,
734 <https://doi.org/10.1016/j.aeolia.2013.09.002>, 2014.

735 Mahowald, N. M., Yoshioka, M., Collins, W. D., Conley, A. J., Fillmore, D. W., and Coleman, D. B.:
736 Climate response and radiative forcing from mineral aerosols during the last glacial maximum, pre-
737 industrial, current and doubled-carbon dioxide climates, *Geophys. Res. Lett.*, 332, 382–385, 2006.

738 Mahowald, N. M., Kloster, S., Engelstaedter, S., Moore, J. K., Mukhopadhyay, S., McConnell, J. R.,
739 Albani, S., Doney, S. C., Bhattacharya, A., Curran, M. A. J., Flanner, M. G., Hoffman, F. M.,
740 Lawrence, D. M., Lindsay, K., Mayewski, P. A., Neff, J., Rothenberg, D., Thomas, E., Thornton, P.
741 E., and Zender, C. S.: Observed 20th century desert dust variability: Impact on climate and
742 biogeochemistry, *Atmos. Chem. Phys.*, 10, 10875–10893, [https://doi.org/10.5194/acp-10-10875-](https://doi.org/10.5194/acp-10-10875-2010)
743 2010, 2010.

744 Miller, R. L. and Tegen, I.: Climate response to soil dust aerosols, *J. Clim.*, 11, 3247–3267,
745 [https://doi.org/10.1175/1520-0442\(1998\)011<3247:CRTSDA>2.0.CO;2](https://doi.org/10.1175/1520-0442(1998)011<3247:CRTSDA>2.0.CO;2), 1998.

746 Nitta, T. and Yamada, S.: Recent warming of tropical sea surface temperature and its relationship to the
747 Northern Hemisphere circulation, *J. Meteorol. Soc. Japan*, 67, 375–383,
748 https://doi.org/10.2151/jmsj1965.67.3_375, 1989.

749 Osborn, T. J., Jones, P. D., Lister, D. H., Morice, C. P., Simpson, I. R., Winn, J. P., Hogan, E., and Harris,

750 I. C.: Land Surface Air Temperature Variations Across the Globe Updated to 2019: The CRUTEM5
751 Data Set, *J. Geophys. Res. Atmos.*, 126, <https://doi.org/10.1029/2019JD032352>, 2021.

752 Pallikari, F.: On the false hypothesis of psi-mediated shift of statistical average in tests with random
753 number generators, in: *The Parapsychological Association Convention 2004*, 157–171,
754 <https://doi.org/10.13140/2.1.4054.5289>, 2004.

755 Parker, D. J., Willetts, P., Birch, C., Turner, A. G., Marsham, J. H., Taylor, C. M., Kolusu, S., and Martin,
756 G. M.: The interaction of moist convection and mid-level dry air in the advance of the onset of the
757 Indian monsoon, *Q. J. R. Meteorol. Soc.*, 142, 2256–2272, <https://doi.org/10.1002/qj.2815>, 2016.

758 Poulsen, O. M., Breum, N. O., Ebbehoj, N., Hansen, A. M., Ivens, U. I., van Lelieveld, D., Malmros, P.,
759 Matthiasen, L., Nielsen, B. H., and Nielsen, E. M.: Sorting and recycling of domestic waste. Review
760 of occupational health problems and their possible causes., *Sci. Total Environ.*, 168, 33–56, 1995.

761 Prospero, J. M. and Nees, R. T.: Impact of the North African drought and El Niño on mineral dust in the
762 Barbados trade winds, *Nature*, 320, 735–738, <https://doi.org/10.1038/320735a0>, 1986.

763 Randles, C. A., Sliva, A. M. da, Buchard, V., Colarco, P., Armenov, A., and Govindaraju, R.: The
764 MERRA-2 Aerosol Reanalysis, 1980 Onward. Part I: System Description and Data Assimilation
765 Evaluation, *J. Clim.*, 30, 6823–6850, <https://doi.org/10.1175/JCLI-D-16-0609.1>, 2017.

766 Rayner, N. A., Parker, D. E., Horton, E. B., Folland, C. K., Alexander, L. V., Rowell, D. P., Kent, E. C.,
767 and Kaplan, A.: Global analyses of sea surface temperature, sea ice, and night marine air temperature
768 since the late nineteenth century, *J. Geophys. Res. Atmos.*, 108, 4407,
769 <https://doi.org/10.1029/2002jd002670>, 2003.

770 Razakov, R. M. and Kosnazarov, K. A.: Dust and salt transfer from the exposed bed of the Aral Sea and
771 measures to decrease its environmental impact, in: *The Aral Sea Basin*, edited by: Micklin, P. P. and
772 Williams, W. D., Springer, Berlin, Heidelberg, 95–102, 1996.

773 Richon, C., Dutay, J., Dulac, F., and Wang, R.: Modeling the biogeochemical impact of atmospheric
774 phosphate deposition from desert dust and combustion sources to the Mediterranean Sea,
775 *Biogeosciences*, 15, 2499–2524, <https://doi.org/10.5194/bg-2017-242>, 2018.

776 Sabeerali, C. T., Ajayamohan, R. S., Bangalath, H. K., and Chen, N.: Atlantic Zonal Mode: An Emerging
777 Source of Indian Summer Monsoon Variability in a Warming World, *Geophys. Res. Lett.*, 46, 4460–

778 4467, <https://doi.org/10.1029/2019GL082379>, 2019.

779 Sanchez de la Campa, A., Garcia-Salamanca, A., Solano, J., de la Rosa, J., and Ramos, J.-L.: Chemical
780 and microbiological characterization of atmospheric particulate matter during an intense African dust
781 event in Southern Spain., *Environ. Sci. Technol.*, 47, 3630–3638, <https://doi.org/10.1021/es3051235>,
782 2013.

783 Schulz, M., Prospero, J. M., Baker, A. R., Dentener, F., Ickes, L., Liss, P. S., Mahowald, N. M., Nickovic,
784 S., García-Pando, C. P., Rodríguez, S., Sarin, M., Tegen, I., and Duce, R. A.: Atmospheric Transport
785 and Deposition of Mineral Dust to the Ocean: Implications for Research Needs, *Environ. Sci.*
786 *Technol.*, 46, 10390–10404, <https://doi.org/10.1021/es300073u>, 2012.

787 Singh, R. P., Prasad, A. K., Kayetha, V. K., and Kafatos, M.: Enhancement of oceanic parameters
788 associated with dust storms using satellite data, *J. Geophys. Res.*, 113, C11008,
789 <https://doi.org/10.1029/2008JC004815>, 2008.

790 Srivastava, G., Chakraborty, A., and Nanjundiah, R. S.: Multidecadal see-saw of the impact of ENSO on
791 Indian and West African summer monsoon rainfall, *Clim. Dyn.*, 52, 6633–6649,
792 <https://doi.org/10.1007/s00382-018-4535-2>, 2019.

793 Storch, H. von and Zwiers, F. W.: *Statistical Analysis in Climate Research*, Cambridge University Press,
794 Cambridge, [https://doi.org/DOI: 10.1017/CBO9780511612336](https://doi.org/DOI:10.1017/CBO9780511612336), 1999.

795 Tegen, I., Lacis, A. A., and Fung, I.: The influence on climate forcing of mineral aerosols from disturbed
796 soils, *Nature*, 380, 419–422, 1996.

797 Tokinaga, H., Richter, I., and Kosaka, Y.: ENSO Influence on the Atlantic Niño, Revisited: Multi-Year
798 versus Single-Year ENSO Events, *J. Clim.*, 32, 4585–4600, 2019.

799 Trenberth, K. E. and Hurrell, J. W.: Decadal atmosphere-ocean variations in the Pacific, *Clim. Dyn.*, 9,
800 303–319, <https://doi.org/10.1007/BF00204745>, 1994.

801 Trenberth, K. E., Dai, A., Van Der Schrier, G., Jones, P. D., Barichivich, J., Briffa, K. R., and Sheffield,
802 J.: Global warming and changes in drought, *Nat. Clim. Chang.*, 4, 17–22,
803 <https://doi.org/10.1038/nclimate2067>, 2014.

804 Veselovskii, I., Goloub, P., Podvin, T., Tanre, D., Da Silva, A., Colarco, P., Castellanos, P., Korenskiy,
805 M., Hu, Q., Whiteman, D. N., Pérez-Ramírez, D., Augustin, P., Fourmentin, M., and Kolgotin, A.:

806 Characterization of smoke and dust episode over West Africa: Comparison of MERRA-2 modeling
807 with multiwavelength Mie-Raman lidar observations, *Atmos. Meas. Tech.*, 11, 949–969,
808 <https://doi.org/10.5194/amt-11-949-2018>, 2018.

809 Wang, B., Wu, R., and Li, T.: Atmosphere-warm ocean interaction and its impacts on Asian-Australian
810 monsoon variation, *J. Clim.*, 16, 1195–1211, [https://doi.org/10.1175/1520-0442\(2003\)16<1195:AOIAII>2.0.CO;2](https://doi.org/10.1175/1520-0442(2003)16<1195:AOIAII>2.0.CO;2), 2003.

812 Wang, L., Chen, W., and Huang, R.: Interdecadal modulation of PDO on the impact of ENSO on the east
813 Asian winter monsoon, *Geophys. Res. Lett.*, 35, <https://doi.org/10.1029/2008GL035287>, 2008.

814 Wang, S., Huang, J., He, Y., and Guan, Y.: Combined effects of the Pacific Decadal Oscillation and El
815 Niño-Southern Oscillation on Global Land Dry-Wet Changes, *Sci. Rep.*, 4, 6651,
816 <https://doi.org/10.1038/srep06651>, 2014.

817 Watanabe, M. and Jin, F. F.: Role of Indian Ocean warming in the development of Philippine Sea
818 anticyclone during ENSO, *Geophys. Res. Lett.*, 29, 1161–1164,
819 <https://doi.org/10.1029/2001gl014318>, 2002.

820 Watanabe, M., Shiogama, H., Tatebe, H., Hayashi, M., Ishii, M., and Kimoto, M.: Contribution of natural
821 decadal variability to global warming acceleration and hiatus, *Nat. Clim. Chang.*, 4, 893–897,
822 <https://doi.org/10.1038/nclimate2355>, 2014.

823 Weare, B. C., Navato, A. R., and Newell, R. E.: Empirical orthogonal analysis of Pacific sea surface
824 temperatures, *J. Phys. Oceanogr.*, 6, 671–678, 1976.

825 Weng, H., Ashok, K., Behera, S. K., Rao, S. A., and Yamagata, T.: Impacts of recent El Niño Modoki
826 on dry/wet conditions in the Pacific rim during boreal summer, *Clim. Dyn.*, 29, 113–129,
827 <https://doi.org/10.1007/s00382-007-0234-0>, 2007.

828 Wu, R. and Kirtman, B. P.: Understanding the impacts of the Indian ocean on ENSO variability in a
829 coupled GCM, *J. Clim.*, 17, 4019–4031, [https://doi.org/10.1175/1520-0442\(2004\)017<4019:UTIOTI>2.0.CO;2](https://doi.org/10.1175/1520-0442(2004)017<4019:UTIOTI>2.0.CO;2), 2004.

831 Wu, X., Liu, J., Wu, Y., Wang, X., Yu, X., Shi, J., and Bi, J.: Aerosol optical absorption coefficients at
832 a rural site in Northwest China : The great contribution of dust particles, *Atmos. Environ.*, 189, 145–
833 152, <https://doi.org/10.1016/j.atmosenv.2018.07.002>, 2018.

834 Xi, X. and Sokolik, I. N.: Dust interannual variability and trend in Central Asia from 2000 to 2014 and
835 their climatic linkages, *J. Geophys. Res. Atmos.*, 120, 12175–12191,
836 <https://doi.org/10.1038/175238c0>, 2016.

837 Yang, S. and Jiang, X.: Prediction of Eastern and Central Pacific ENSO Events and Their Impacts on
838 East Asian Climate by the NCEP Climate Forecast System, *J. Clim.*, 27, 4451–4472,
839 <https://doi.org/10.1175/JCLI-D-13-00471.1>, 2014.

840 Yang, X. and Huang, P.: Restored relationship between ENSO and Indian summer monsoon rainfall
841 around 1999/2000, *Innov.*, 2, 100102, <https://doi.org/10.1016/j.xinn.2021.100102>, 2021.

842 Yu, J.-Y., Mechoso, C. R., McWilliams, J. C., and Arakawa, A.: Impacts of the Indian Ocean on the
843 ENSO cycle, *Geophys. Res. Lett.*, 29, 1204, 2002.

844 Yu, J. and Kao, H.: Decadal changes of ENSO persistence barrier in SST and ocean heat content indices :
845 1958 – 2001, *J. Geophys. Res.*, 112, 1–10, <https://doi.org/10.1029/2006JD007654>, 2007.

846 Yu, Y., Notaro, M., Liu, Z., Wang, F., Alkolibi, F., Fadda, E., and Bakhrjy, F.: Climatic controls on the
847 interannual to decadal variability in Saudi Arabian dust activity: Toward the development of a
848 seasonal dust prediction model, *J. Geophys. Res. Atmos.*, 120, 1739–1758,
849 <https://doi.org/10.1002/jgrc.20224>, 2015.

850 Yuan, Y. and Yang, S.: Impacts of Different Types of El Niño on the East Asian Climate: Focus on
851 ENSO Cycles, *J. Clim.*, 25, 7702–7722, 2012.

852